

Engineered Randomness for Ubiquitous Quantum-Enhanced Metrology in Exponential-Dimensional Manifolds

Yaoming Chu^{1,2}, Baiyi Yu^{3,4,1}, Hartmut Häffner^{3,4},
Markus Heyl^{5,6}, Nathan Goldman^{7,8,9}, Jianming Cai^{1,2,*}

¹ Center for Intelligence and Quantum Science (CIQS),

International Joint Laboratory on Quantum Sensing and Quantum Metrology, School of Physics,

Huazhong University of Science and Technology, Wuhan 430074, China.

²Hubei Key Laboratory of Gravitation and Quantum Physics,

Institute for Quantum Science and Engineering,

Huazhong University of Science and Technology, Wuhan 430074, China.

³Department of Physics, University of California, Berkeley, CA 94720, USA.

⁴Challenge Institute for Quantum Computation, University of California, Berkeley, CA 94720, USA.

⁵Theoretical Physics III, Center for Electronic Correlations and Magnetism, Institute of Physics,

University of Augsburg, Universitätsstr. 12a, 86159 Augsburg, Germany.

⁶Centre for Advanced Analytics and Predictive Sciences (CAAPS),

University of Augsburg, Universitätsstr. 12a, 86159 Augsburg, Germany.

⁷CENOLI, Université Libre de Bruxelles, CP 231, Campus Plaine, B-1050 Brussels, Belgium

⁸International Solvay Institutes, 1050 Brussels, Belgium

⁹Laboratoire Kastler Brossel, Collège de France, CNRS,

ENS-Université PSL, Sorbonne Université, 11 Place Marcelin Berthelot, 75005 Paris, France

*Corresponding author. Email: jianmingcai@hust.edu.cn

The exponential growth of many-body Hilbert space presents a fundamental barrier to quantum technology, obscuring the search for physically significant states within an astronomically vast landscape. Consequently, resources for quantum-enhanced metrology have been largely confined to the symmetric subspace whose dimensionality scales only polynomially with the particle number—leaving the vast majority of the Hilbert space largely unexplored and poorly understood. Here we challenge this paradigm by demonstrating that metrological advantage can arise as a ubiquitous feature across exponential-dimensional manifolds. By tailoring the first-moment structure of random unitaries, we uncover dense manifolds of engineered random states (ERSs) where Heisenberg-limited scaling emerges as a statistically generic property. This ubiquity endows these resource states with inherent resilience against parameter disorder. We experimentally validate this framework on a trapped-ion processor, achieving a metrological enhancement of 6.98 ± 0.38 dB beyond the standard quantum limit. Potential applications extend to diverse platforms, ranging from superconducting circuits and waveguide QED to solid-state spins and polar molecules. Our results establish a powerful paradigm where quantum-enhanced precision can be harvested from the exponential vastness of the Hilbert space.

The dimension of a quantum system’s Hilbert space grows exponentially with the number of particles N , quickly becoming astronomically vast (1): for $N = 300$ qubits, the 2^{300} available basis states already exceed the estimated number of atoms in the observable universe. This exponential complexity provides the foundation for many-body physics and quantum-enhanced technologies, yet simultaneously defines the central challenge for navigating and exploring this space to find states with useful properties. At a more fundamental level, uncovering the underlying structure of the Hilbert space—its geometry (2, 3) and governing constraints (4–6)—and identifying its physically significant manifolds stand as a critical frontier.

Historically, the search for metrologically useful states has largely centered on the symmetric subspace (7, 8), yielding canonical resources such as Dicke (9), Greenberger-Horne-Zeilinger (GHZ) (10) and squeezed states (11). Although quantum advantage is identified within this narrow niche of polynomial dimensionality (12), generic many-body states in the exponentially vast Hilbert

space are widely believed to offer little metrological usefulness. Known exceptions—for example, ground states of specific local Hamiltonians (13–15) or states generated through fine-tuned quantum evolution (16–21)—are rare and exist only as isolated singularities. These facts conceptually raise a pivotal question: *Does the Hilbert space embody structured manifolds where quantum advantage ubiquitously persists across much higher—potentially even exponential—dimensions?*

Here, we show that physically significant manifolds, which enables quantum-enhanced metrology to surpass the standard quantum limit (SQL), can be identified by leveraging cleverly engineered randomness across the Hilbert space. Specifically, by shaping the first moments of unitary ensembles beyond the trivial Haar-randomness (12, 22), we theoretically find that Heisenberg-limited (HL) scaling—representing a fundamental $N^{1/2}$ precision enhancement over the SQL—unexpectedly emerges as a statistically generic property of exponential-dimensional manifolds (see Figure 1a). Our findings affirmatively answer the posed question that quantum advantage is not a rare, symmetry-protected exception, but a ubiquitous feature that permeates the exponential reaches of the Hilbert space via engineered randomness.

We experimentally validate quantum-enhanced metrology on a trapped-ion processor, achieving a phase measurement gain of 6.98(\pm 0.38) dB beyond the SQL using 10-qubit engineered random states (ERSs). Crucially, we find that metrological advantage is a universal attribute of the ERS manifold, granting the strategy remarkable robustness against parameter disorder that otherwise severely degrades conventional protocols for resource state generation. These results not only substantially broaden the scope of quantum metrology, but also illuminate our understanding of the fundamental geometry of entanglement and the structural landscape of many-body quantum states. Our work thus opens an avenue toward efficient harvesting of useful states from the exponentially vast Hilbert space through properly engineered randomness.

Main result

To set the stage, we investigate a generic quantum system composed of N particles, each equipped with a local Hilbert space of dimension d . The power of quantum metrology is fundamentally dictated by how distinguishable a quantum state becomes under the continuous encoding of a parameter ϑ . This distinguishability is rigorously quantified by the quantum Fisher information

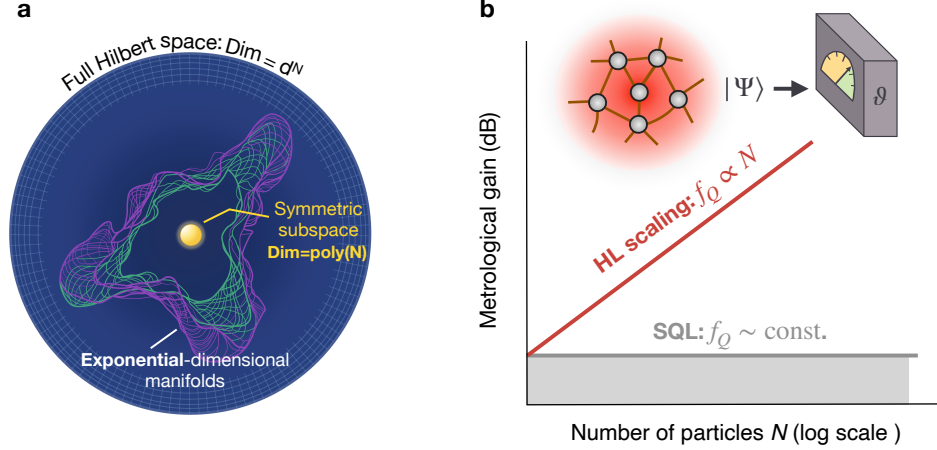


Figure 1: Quantum-enhanced metrology from the exponentially vast Hilbert space. (a) Generic Haar-random states offer negligible metrological usefulness, thus it is critical to identify the structured manifolds embedded in the Hilbert space that yield quantum advantage. (b) The metrological usefulness of an input state $|\Psi\rangle$ for estimating a parameter ϑ is quantified by the QFI density, $f_Q = F_Q/N$, which determines the fundamental precision floor via the quantum Cramér-Rao bound, $\delta\vartheta \geq (Nf_Q)^{-1/2}$. The constant ($f_Q \sim \text{const.}$) and linear growth ($f_Q \propto N$) behaviors correspond to the SQL and Heisenberg-limited (HL) scalings, respectively.

(QFI), $F_Q[\rho; O]$, a metric that defines the distance between an input state ρ and its parameter-translated counterpart $e^{-i\vartheta O} \rho e^{i\vartheta O}$ (8, 23). Here, O is the Hermitian generator associated with the translation of ϑ ; without loss of generality, we adopt a local generator: $O = \sum_{m=1}^N O_m$, where the operator O_m acting on the m -th particle has a spectrum of unit width. For a pure state $\rho = |\Psi\rangle\langle\Psi|$, the QFI is determined by its susceptibility to the generator O , yielding the elegantly simple form as follows

$$F_Q(|\Psi\rangle; O) = 4 \left(\langle\Psi|O^2|\Psi\rangle - \langle\Psi|O|\Psi\rangle^2 \right). \quad (1)$$

The operational significance of the QFI lies in its direct relation to the ultimate metrological performance: it establishes a fundamental limit on the achievable precision, $\delta\vartheta$, via the so-called quantum Cramér-Rao bound, $(\delta\vartheta)^{-2} \leq F_Q[|\Psi\rangle; O]$ (23). Crucially, the QFI also connects metrological precision directly to the depth of multipartite entanglement. A QFI density $f_Q = F_Q/N$ exceeding an integer k verifies that the system possesses at least $(k + 1)$ -partite entanglement (24–29). Consequently, achieving HL precision ($F_Q \propto N^2$) strictly requires genuine multipartite entanglement,

characterized by an extensive QFI density $f_Q \propto N$ (see Figure 1b).

Below, we demonstrate—through two key findings—that many-body states generated via properly engineered randomness can generically unlock the HL precision scaling from the exponentially vast Hilbert space. Specifically, our framework generates metrological states by evolving an initial state $|\Psi\rangle$ under a unitary transformation U . Without loss of generality, hereafter $|\Psi\rangle$ is assumed to be a N -particle product state: $|\Psi\rangle = \otimes_{m=1}^N |\psi\rangle_m$, where each component is the eigenstate of the local traceless Hermitian generator O_m with a positive eigenvalue λ , i.e. $O_m |\psi\rangle_m = \lambda |\psi\rangle_m$. Our first finding is a class of α -random unitary ensembles—denoted by \mathcal{U}_α —that are distinguished by the characteristic first-moment structure

$$\mathbb{E}_{U \sim \mathcal{U}_\alpha} [U_{i_1 j_1} U_{i_2 j_2}^*] = \alpha \delta_{i_1 j_1} \delta_{i_2 j_2} + (1 - \alpha) \Delta_{i_1, i_2, j_1, j_2}. \quad (2)$$

Here, $\alpha \in (0, 1)$ is the defining parameter of the ensemble, and the second term corresponds to a completely depolarizing channel for a quantum operator \mathcal{A} ,

$$\mathcal{D}(\mathcal{A}) \equiv \sum_{i_1 i_2 j_1 j_2} \Delta_{i_1, i_2, j_1, j_2} \mathcal{A}_{i_2 i_1} |j_2\rangle \langle j_1| = c \frac{\mathbb{I}}{D}, \quad (3)$$

where the constant $c = \text{tr}(\mathcal{A})$ is fixed by invoking the unitarity of U (30), and $D = d^N$ is the Hilbert space dimension. Crucially, α -random unitary ensembles have a unique feature, as stated in the following lemma.

Lemma 1 *An α -random unitary ensemble \mathcal{U}_α contracts a quantum operator \mathcal{A} by a factor of α in an average sense*

$$\mathbb{E}_{U \sim \mathcal{U}_\alpha} [U^\dagger \mathcal{A} U] = \alpha \mathcal{A} + (1 - \alpha) \text{tr}(\mathcal{A}) \frac{\mathbb{I}}{D}. \quad (4)$$

In contrast to the standard Haar-randomness leading to $\alpha = 0$, our engineered randomness breaks this triviality by introducing the first α -contraction term [with $\alpha \in (0, 1)$] for arbitrary quantum operators. This non-trivial universal contraction is the key mechanism essentially underlying the emergence of a HL precision scaling achieved by the generated ERSs. As an illustrative example, we consider a N -qubit system initially prepared in a fully polarized state along the z axis (i.e. $|\Psi\rangle = |0\rangle^{\otimes N}$) and take the local Hermitian generator associated with the parameter change as $O_m = \sigma_z^{(m)}/2$, where $\sigma_\mu^{(m)}$ with $\mu = x, y, z$ are Pauli operators supported on the m -th qubit. Applying random unitaries from \mathcal{U}_α contracts the expectation values of $J_z = \sum_{m=1}^N \sigma_z^{(m)}/2$ and J_z^2

by a factor of α based on Lemma 1. Therefore, the two terms in Eq. (1) for $O = J_z$ are reduced by α and α^2 , yielding an average QFI of $\alpha(1 - \alpha)N^2 + O(N)$ that reaches the HL scaling.

The result is rigorously formalized in the following theorem, with proofs outlined in the Appendix and detailed in the Supplementary Materials (30).

Theorem 1 *Let $|\Psi_U\rangle = U|\Psi\rangle$ be the family of ERSs generated by U from an α -random unitary ensemble \mathcal{U}_α . Then, the quantum Fisher information of these states associated with the generator $O = \sum_{m=1}^N O_m$ attains the following ensemble average,*

$$\mathbb{E}_{U \sim \mathcal{U}_\alpha} [F_Q(|\Psi_U\rangle; O)] = 4\alpha(1 - \alpha)\lambda^2 N^2 + \Theta(N), \quad (5)$$

provided that the variance of $f_U = \langle \Psi_U | O | \Psi_U \rangle$ scales at most as $\Theta(N)$, namely $\mathbb{E}_{U \sim \mathcal{U}_\alpha} [f_U^2] - \mathbb{E}_{U \sim \mathcal{U}_\alpha}^2 [f_U] \leq \Theta(N)$. Here, $\Theta(\xi)$ indicates an asymptotic scaling identical to ξ for large ξ .

Importantly, Theorem 1 establishes a principled and systematic route toward ERS manifolds with superior average metrological usefulness. We emphasize that these ERSs are largely disjoint from the symmetric subspace (30), thus representing fundamentally new types of metrologically useful states. Building upon this framework, we next turn to present our second key finding, which addresses the distribution of ERS performance by revealing a striking concentration-of-measure phenomenon in high-dimensions: the QFI of most ERSs generated by the α -random unitary ensemble can cluster within a thin shell around their average.

Theorem 2 *Under the same setting of Theorem 1, the quantum Fisher information of ERSs generated by an α -random unitary ensemble concentrates to the Heisenberg-limited scaling,*

$$\Pr \left(F_Q(|\Psi_U\rangle; O) < \Theta(N^2) \right) \leq \exp \left(-\Theta \left(\frac{D}{\text{poly}(N)} \right) \right), \quad (6)$$

provided that the expectation value function $f(U; \mathcal{A}) = \langle \Psi_U | \mathcal{A} | \Psi_U \rangle$ for $\mathcal{A} \in \{O, O^2\}$ is $L_{\mathcal{A}}$ -Lipschitz continuous and satisfies the following inequality for $\forall \epsilon > 0$,

$$\Pr \left(|f(U; \mathcal{A}) - \mathbb{E}_{U \sim \mathcal{U}_\alpha} [f(U; \mathcal{A})]| \geq \epsilon \right) \leq 2 \exp \left(-\frac{c\epsilon^2}{L_{\mathcal{A}}^2} \right), \quad (7)$$

where the probability $\Pr(\cdot)$ is taken over \mathcal{U}_α and c represents a universal positive constant with the ratio $c/L_{\mathcal{A}}^2 = \Theta(D/\text{poly}(N))$. Here, the symbol $\text{poly}(\cdot)$ denotes an arbitrary polynomial.

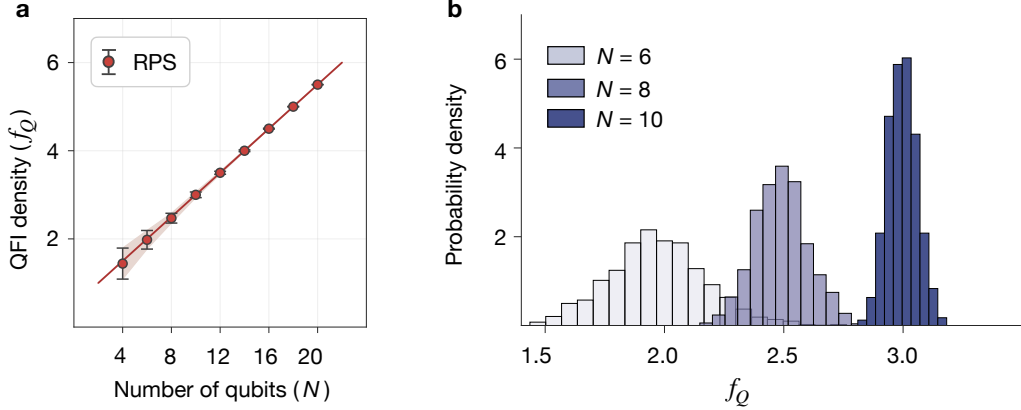


Figure 2: Heisenberg-limited scaling emerging from engineered random unitary ensembles.

(a) At $\alpha = 1/2$, the average QFI densities for RPSs—a specific example of ERSs—exhibit excellent agreement with the theoretical prediction of HL scaling $\mathbb{E}[f_Q] = N/4 + 1/2$ (solid line). Each data point represents an average over 200 exact random numerical realizations. The shaded regions denote the statistical spread, which rapidly diminishes with system size, revealing the concentration-of-measure phenomenon. (b) Probability density distributions from 2000 realizations at different system sizes further highlight the concentration of f_Q in high dimensions.

We remark that the condition in Eq. (7) reflects a generic and fundamental feature of high-dimensional ensembles, which can be rigorously established for diverse measures with positive Ricci curvature (31–33). Theorem 2 demonstrates that the ERSs generated by α -random unitary ensembles constitute a physically significant manifold within the Hilbert space for quantum-enhanced metrology, and the probability of encountering a ERS that cannot achieve the HL scaling is exponentially vanishing. Together with Theorem 1, it leads to our main result that *many-body ERSs are capable of generically achieving enhanced precision at the Heisenberg-limited scaling*. This suggests that metrologically useful states are not rare, fine-tuned anomalies; rather, they can emerge as typical outcomes when sampling from certain manifolds in the Hilbert space.

Examples of ERS manifolds

Theorem 1 and 2 provide a guiding framework for finding Heisenberg-limited ERS manifolds in the exponentially vast Hilbert space. To demonstrate the feasibility of α -random unitary ensembles

to generate metrologically useful ERSs, we treat the general form of a unitary operator U via a similarity transformation,

$$U = V\Phi V^\dagger, \quad (8)$$

where V and Φ denote the transformation and core unitaries, respectively. We next present two explicit examples of α -random unitary ensembles that satisfy the prescribed first-moment statistical identities in Eq. (2).

Random phase state

The first example is a simple and interesting class of metrologically useful states of a N -qubit system, namely the random phase states (RPSs), written as

$$|\Psi(\varphi_1, \dots, \varphi_D)\rangle = \frac{1}{\sqrt{D}} \sum_{b=1}^D e^{i\varphi_b} |b\rangle, \quad (9)$$

where $\{|b\rangle\}_{b=1}^D$ spans the computational basis and $\{\varphi_b\}_{b=1}^D$ is a set of independent random phases. The RPSs are generally believed to offer no quantum advantage. Surprisingly, we will show that they can in fact serve as a potent resource for achieving the HL precision scaling.

Starting from an initial product state aligned along the x -axis, namely $|\Psi\rangle = |\mathbf{x}\rangle = |+\rangle^{\otimes N}$, RPSs can be generated via a diagonal α -random unitary ensemble, $\Phi = \text{diag}[\{e^{i\varphi_b}\}_{b=1}^D]$, where each random phase is drawn independently from a distribution $p(\varphi_b)$. The corresponding ensemble contraction factor [see Eq. (2)], is given by (30)

$$\sqrt{\alpha} = \mathbb{E}_{\varphi_b \sim p(\varphi_b)} [\exp(i\varphi_b)]. \quad (10)$$

Theorem 1 guarantees that the ensemble-averaged QFI exhibits HL scaling as long as the factor α lies within $(0, 1)$. Rather than adopting the conventional unitary ensemble (34) with each phase uniformly distributed within $[0, 2\pi]$ that trivially results in $\alpha = 0$, we consider a general normal distribution, for which $\alpha = \exp(-\sigma^2)$ with σ the standard deviation of φ_b .

We further establish the typicality of HL scaling by situating this RPS class within the geometry of high-dimensional Gaussian measure spaces. Identifying the collective spin operator J_x as the generator of parameter change, we explicitly evaluate the concentration behavior in Eq. (7) for $\mathcal{A} \in \{J_x, J_x^2\}$. It can be shown that $c \propto \sigma^{-2}$, while the Lipschitz constants are upper bounded

by $L_{\mathcal{A}} \leq N^\gamma/D^{1/2}$ with $\gamma = 1$ and 2 , respectively (30). Consequently, Theorem 2 ensures the tight concentration of the QFI at its mean, establishing the metrological advantage as a ubiquitous property of the entire RPS manifold (see Figure 2), as stated by the following corollary.

Corollary 2.1 *For any $\alpha \in (0, 1)$, nearly all random phase states can achieve quantum-enhanced precision at the Heisenberg-limited scaling.*

Remarkably, we can also rigorously prove that the RPS manifold necessitates an exponential embedding dimension of 2^N ; namely, it cannot be confined to any Hilbert subspace of dimension smaller than 2^N (30, 35). This fact signifies that the RPS manifold exploits the full exponential complexity of the Hilbert space—a stark departure from the polynomial constraints of the conventional symmetric subspace.

Chimera-superposition states

We apply our findings to the second example with the transformation unitaries V in Eq. (8) chosen to be Haar-random on the special unitary group $SU(D)$ (22). Interestingly, the class of states generated from this Haar-random construction admit the following decomposition,

$$|\Psi_U\rangle = \sqrt{\alpha}e^{i\beta}|\Psi\rangle + \sqrt{1-\alpha}|\Psi_H^{(1)}\rangle, \quad (11)$$

with $\beta = \arg[\text{tr}(\Phi)]$, and the contraction factor α [see Eq. (2)] is given by

$$\alpha = \frac{1}{D}|\text{tr}(\Phi)|^2. \quad (12)$$

The first component $|\Psi\rangle$ represents the initial product state. The second component, $|\Psi_H^{(1)}\rangle$, exhibits first-order Haar-randomness, characterized by vanishing polarization along any arbitrary directions. This component can be further generalized to be exact Haar-random states (30). The resulting states therefore embody a new form of quantum superposition, intertwining an ordered contribution (such as fully polarized states) with a highly-random part. We thus designate these configurations as *Chimera-superposition states* (CSSs).

The two constituents of a CSS differ markedly in their physical character—for instance, in state complexity (3, 36)—and cannot be connected through simple observables such as $\mathcal{A} = J_z$

or $\mathcal{A} = J_z^2$, namely $|\langle \Psi | \mathcal{A} | \Psi_H^{(1)} \rangle|^2 = \Theta(1/D)$ (30). As a consequence, expectation values of such observables can be approximated as

$$\langle \Psi_U | \mathcal{A} | \Psi_U \rangle \approx \alpha \langle \Psi | \mathcal{A} | \Psi \rangle + (1 - \alpha) \langle \Psi_H^{(1)} | \mathcal{A} | \Psi_H^{(1)} \rangle, \quad (13)$$

which is naturally consistent with the operator contraction in Lemma 1, since the second term on the right-hand side is typically negligible. Building on Theorem 1 and 2, we can similarly extend the concentration of superior metrological usefulness to this CSS manifold by identifying $c = D/4$ and $L_{\mathcal{A}} \propto \text{poly}(N)$ for $\mathcal{A} \in \{J_z, J_z^2\}$ [see Eq. (7)] under the Haar measure on $SU(D)$.

Corollary 2.2 *For any $\alpha \in (0, 1)$, nearly all Chimera-superposition states can achieve quantum-enhanced precision at the Heisenberg-limited scaling.*

This corollary provides a solid mathematical foundation for the ubiquitous quantum advantage inherent to the CSS manifold. It rigorously establishes that the metrological usefulness often attributed to complex scrambling dynamics (37–39) is, in fact, a generic feature of engineered randomness. Similar results can be extended to the Gaussian unitary ensembles (30, 40, 41). Notably, similar to the RPSs, this CSS manifold also possesses an embedding dimension of $D = d^N$, matching the full exponential complexity of the Hilbert space (30).

Experimental verification of enhanced metrology using ERSs

Guided by the generic usefulness established for the RPS manifold, we extend our analysis to an easily accessible class of ERSs within N -qubit experimental platforms. Specifically, we consider a random Hamiltonian ensemble restricted to at most two-body Ising interactions,

$$H = \sum_{(ij) \in e^*} \phi_{ij} \left(\sigma_z^{(i)} \sigma_z^{(j)} - \sigma_z^{(i)} - \sigma_z^{(j)} \right), \quad (14)$$

where e^* denotes the edge set of a star configuration. Each interaction weight ϕ_{ij} is independently sampled from a normal distribution with zero mean and a standard deviation such that $\mathbb{E}[\exp(4i\phi_{ij})] \ll 1$. These weights are mapped to the phases $\{\varphi_b\}$ in Eq. (9) via a $D \times (N - 1)$ linear transformation matrix (30). Start from an initial state $|\mathbf{x}\rangle = |+\rangle^{\otimes N}$, we apply the unitaries

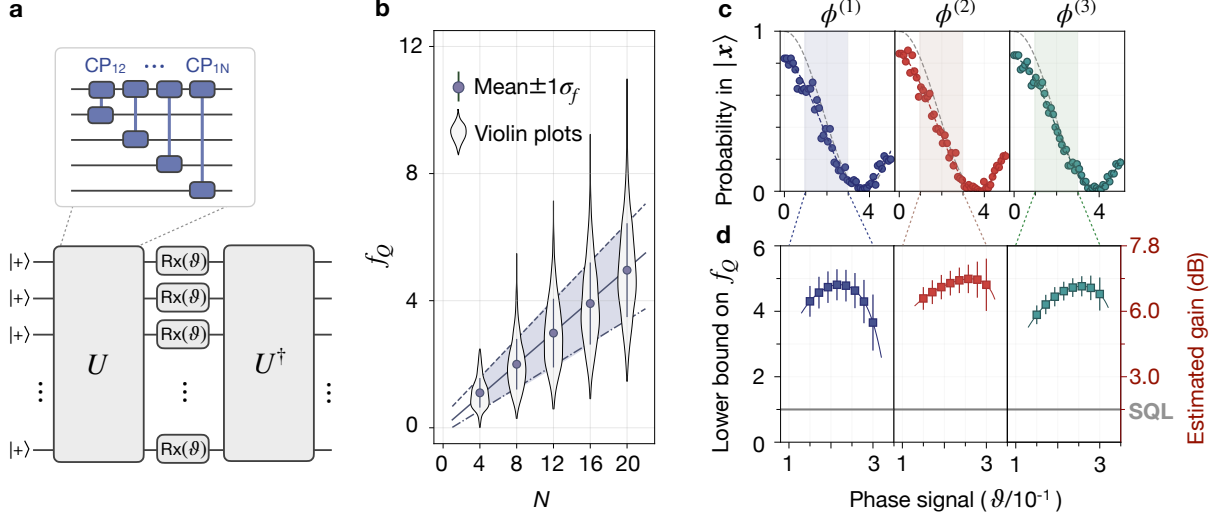


Figure 3: Quantum-enhanced metrology using ERSs in a trapped-ion platform. (a) Time-reversal sensing protocol with ERSs created by random quantum circuits (RQCs) consisting of two-qubit CP gates (see Appendix). (b) Violin plots of f_Q for varying system sizes, each based on 2000 random numerical realizations of the ERS. Mean values (filled circles) agree well with $\mathbb{E}[f_Q] = N/4$ (solid line), while $\mathbb{E}[f_Q] \pm \sigma_f$ also exhibit linear scaling with slopes 0.30 (dashed) and 0.18 (dash-dotted). (c) Three 10-qubit RQCs, with different random interaction weights [see Eq. (14) and Appendix], are executed on IonQ’s Forte-1 processor. After phase encoding and time reversal, the return probability $P(\vartheta)$ is recorded as a function of ϑ . (d) The lower bound on f_Q of the experimentally generated ERS are inferred from the measured phase uncertainty. The corresponding metrological gain beyond the SQL is indicated, showing the quantum enhancement achievable with these states. In all panels, a standard deviation of $\sigma_\phi = 0.5\pi$ is set for the interaction weight parameters.

$U = \exp(iH)$ via the random quantum circuits (RQCs) in Figure 3a. This procedure generates random weighted graph states (42)—which essentially constitute a specific realization of the broader RPS class characterized by correlated random phases (30). We show in what follows that these ERSs also possess a significant metrological potential that has surprisingly remained hitherto unexplored. It is worth to emphasize that the mutual commutativity of all terms in Eq. (14) in principle allows for the parallel execution of all two-qubit entangling operations. Thus, this offers a scalable route toward the rapid preparation of large-scale ERSs achieving Heisenberg-limited quantum

measurement precision (43).

Numerical simulations spanning a large number of such RQCs, presented in Figure 3b, reveal that a predominant fraction of the resulting states displays genuine metrological advantage: their QFI densities significantly exceed the SQL (i.e. $f_Q = 1$) and the ensemble average follows the theoretical scaling of $\mathbb{E}[f_Q] = N/4$ (30). Crucially, while these circuit-generated ERSs differ from the exact RPS class due to correlations among random phases, the ± 1 standard deviation bounds still faithfully maintain the HL scaling (30). This statistical spread also enables the efficient identification of a significant subset of ERSs with QFI densities well beyond the ensemble average.

In our experiments, we create three instances of such 10-qubit ERSs with distinct sets of random interaction weights on an IonQ trapped-ion processor, and demonstrate quantum-enhanced metrology by exploiting a time-reversal protocol (44, 45). In this protocol, the prepared ERS undergoes a collective phase shift $e^{i\vartheta J_x}$, where ϑ represents the parameter to be estimated, modeling the signal accumulated from an external field coupled to the probe in a standard sensing scenario. Following this interrogation stage, a time-reversed circuit U^\dagger is applied to unravel the engineered correlations and convert the accumulated phase into a measurable population signal. The measured probabilities $P(\vartheta)$, of which the system returns to $|\mathbf{x}\rangle$, are presented in Figure 3c. From the regions of $P(\vartheta)$ with large slopes versus ϑ , we extract a metrological gain of $6.98(\pm 0.38)$ dB beyond the SQL, giving rise to apparent quantum enhancement, as detailed in Figure 3d. We note that the realized ERSs are mixed states due to inevitable decoherence within the real quantum device. Their QFI exhibits a highly nonlinear and intricate dependence on the underlying density matrix (24, 30), rendering the direct evaluation intractable. In this situation, the observed measurement precision therefore provides a certified lower bound on the QFI density of these ERSs, as dictated by the quantum Cramér-Rao bound—which holds universally for both pure and mixed states (23).

Metrological resilience against parameter disorder

In contrast to conventional protocols, where metrological usefulness hinges on a singular configuration, the ERS generation affords substantial experimental flexibility by exploiting the typicality of HL scaling over a dense region of Hilbert space. Numerical results of Figure 4 illustrate this metrological resilience by examining the effect of parameter disorder on the ERS framework and

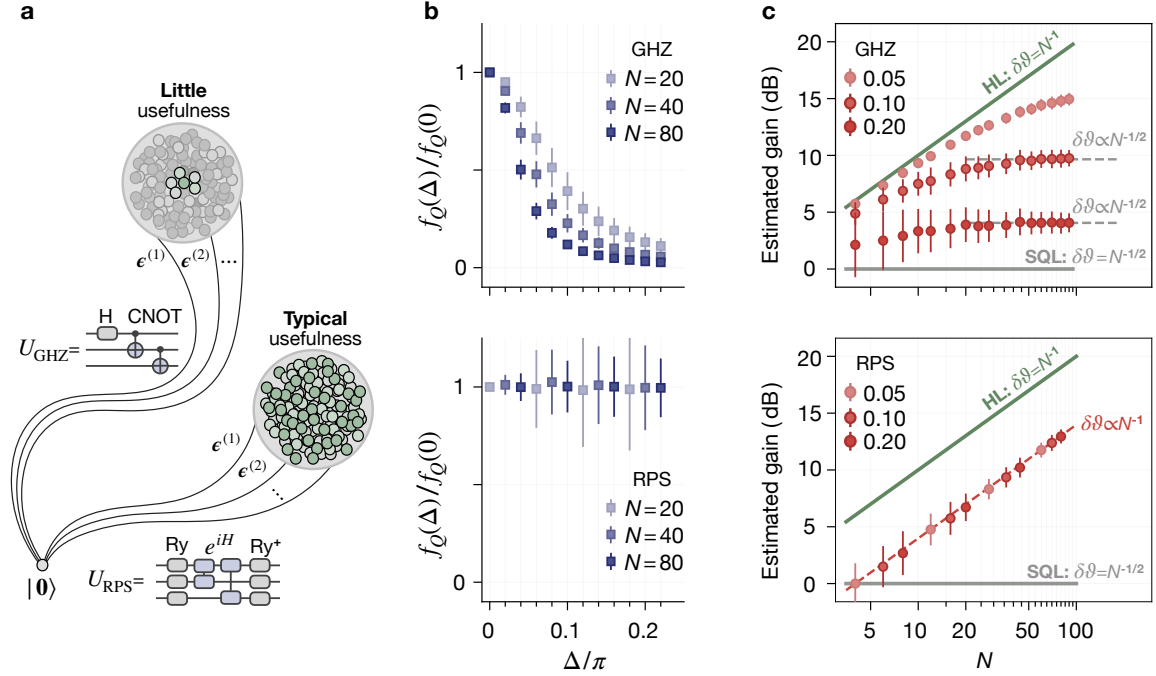


Figure 4: Numerical analysis of metrological resilience against parameter disorder. (a) Schematic of parameter disorder (denoted by ϵ) introduced into the two-qubit CNOT gates for GHZ-state preparation and the Hamiltonian interaction weights [see Eq. (14)] for ERS generation. Each random instance is independently sampled from a normal distribution $\mathcal{N}(0, \Delta^2)$. (b) Normalized QFI density (relative to the ideal case of $\epsilon = 0$) as a function of the disorder strength Δ . The traditional protocol for the GHZ state generation exhibits a marked deterioration, whereas the performance of the ERS framework remains essentially invariant, demonstrating near-complete resilience to parameter disorder. (c) Scaling of the metrological gain (estimated from the QFI) with the system size N . Symbols and curves from light to dark shades represent $\Delta/\pi = 0.05, 0.1, 0.2$, with upper and lower panels corresponding to the GHZ and ERS scenarios respectively. For a fixed Δ , the extracted gain of the perturbed GHZ states ceases to grow at large N , eventually falling back to the SQL yielding a precision of $\delta\theta \propto N^{-1/2}$. In stark contrast, the generated ERSs maintain the characteristic HL scaling ($\delta\theta = 2N^{-1}$) even under substantial disorder.

the canonical GHZ-state preparation protocol. As examples, we consider the CNOT gates used for the GHZ state varied as $\text{CNOT}^{(\epsilon)} = \exp[-i(\pi/4 + \epsilon_i)\sigma_z^{(i)}\sigma_x^{(i+1)}] \exp[i\pi(\sigma_z^{(i)} + \sigma_x^{(i+1)})/4]$ (46, 47), while the interaction weights in Eq. (14) for ERS creation are perturbed according to $\phi_{ij}^{(\epsilon)} = \phi_{ij} + \epsilon_{ij}$, with the baseline parameters $\{\phi_{ij}\}$ yielding a QFI density near the ensemble average to characterize

the typical feature of the ERSs. Here, all perturbation parameters ϵ_i and ϵ_{ij} are independently drawn from a normal distribution with zero mean and standard deviation Δ . With increasing Δ , the estimated metrological gain of the perturbed GHZ states is severely compromised, causing the scaling to revert from the HL toward the SQL at large N . In sharp contrast, the generation of metrologically useful ERSs rarely degrades even under substantial disorder in ϕ_{ij} , consistently preserving the predicted HL scaling. Crucially, as detailed in Supplementary Materials (30), we analytically prove that this resilience would be a universal feature of the ERS generation, independent of the specific disorder distribution. Such inherent resilience—particularly in the large-system limit—positions the present framework as a promising candidate for architectures plagued by parameter inhomogeneity. Potential applications range from superconducting circuits with non-uniform couplings and calibration offsets (48, 49) to disordered platforms like waveguide QED systems (50, 51), solid-state spins (52, 53) and ultracold polar molecules (54) where positional and interaction randomness are often intrinsic constraints.

Summary and outlook

Our work fundamentally shifts the paradigm for accessing quantum advantage in metrology by uncovering physically significant manifolds hidden within the deep Hilbert space via engineered randomness. In particular, we demonstrate that Heisenberg-limited scaling can be ubiquitously unlocked in exponential-dimensional manifolds. It challenges the long-standing consensus that many-body entangled states capable of offering quantum advantage are exceptional and restricted to the symmetric subspace of polynomial dimensionality. This finding establishes engineered randomness as a guiding principle for navigating the extremely challenging, exponentially complex Hilbert space, offering a versatile framework to probe its underlying geometry and structure while pushing the boundaries of both quantum information science and many-body physics.

Looking forward, our results open several compelling avenues extending far beyond metrology. The utility of our framework rests on the QFI, which serves dual roles as a metrological figure of merit and a rigorous witness of genuine multipartite entanglement (24), a central yet elusive resource in quantum many-body physics (55). Transcending a sole focus on the QFI, incorporating complementary metrics—such as the geometric measure of entanglement (56, 57) or contextuality

(58)—might further illuminate additional physically significant regions of the Hilbert space. The framework of engineered randomness also suggests a new strategy for quantum circuit design: rather than aiming for Haar randomness (59, 60), one could possibly tailor the measure over circuit parameter spaces to steer quantum evolutions toward valuable sectors of the Hilbert space.

References and Notes

1. R. P. Feynman, Simulating physics with computers. *Int. J. Theor. Phys.* **21**, 467–488 (1982), <https://doi.org/10.1007/BF02650179>.
2. M. A. Nielsen, M. R. Dowling, M. Gu, A. C. Doherty, Quantum Computation as Geometry. *Science* **311**, 1133–1135 (2006), <http://dx.doi.org/10.1126/science.1121541>.
3. A. R. Brown, A quantum complexity lower bound from differential geometry. *Nat. Phys.* **19**, 401–406 (2023), <https://www.nature.com/articles/s41567-022-01884-6>.
4. E. H. Lieb, D. W. Robinson, The finite group velocity of quantum spin systems. *Commun. Math. Phys.* **28**, 251–257 (1972), <https://doi.org/10.1007/BF01645779>.
5. J. Eisert, M. Cramer, M. B. Plenio, Colloquium: Area laws for the entanglement entropy. *Rev. Mod. Phys.* **82**, 277–306 (2010), <https://link.aps.org/doi/10.1103/RevModPhys.82.277>.
6. L. Lami, B. Regula, No second law of entanglement manipulation after all. *Nat. Phys.* **19**, 184–189 (2023), <http://dx.doi.org/10.1038/s41567-022-01873-9>.
7. C. L. Degen, F. Reinhard, P. Cappellaro, Quantum sensing. *Rev. Mod. Phys.* **89**, 035002 (2017), <https://link.aps.org/doi/10.1103/RevModPhys.89.035002>.
8. L. Pezzè, A. Smerzi, M. K. Oberthaler, R. Schmied, P. Treutlein, Quantum metrology with nonclassical states of atomic ensembles. *Rev. Mod. Phys.* **90**, 035005 (2018), <https://link.aps.org/doi/10.1103/RevModPhys.90.035005>.
9. R. H. Dicke, Coherence in Spontaneous Radiation Processes. *Phys. Rev.* **93**, 99–110 (1954), <https://link.aps.org/doi/10.1103/PhysRev.93.99>.

10. D. M. Greenberger, M. A. Horne, A. Zeilinger, Going Beyond Bell's Theorem, in *Bell's Theorem, Quantum Theory and Conceptions of the Universe* (Dordrecht), pp. 69–72 (1989), https://doi.org/10.1007/978-94-017-0849-4_10.
11. M. Kitagawa, M. Ueda, Squeezed spin states. *Phys. Rev. A* **47**, 5138–5143 (1993), <https://link.aps.org/doi/10.1103/PhysRevA.47.5138>.
12. M. Ozszmaniec, *et al.*, Random Bosonic States for Robust Quantum Metrology. *Phys. Rev. X* **6**, 041044 (2016), <https://link.aps.org/doi/10.1103/PhysRevX.6.041044>.
13. I. Frérot, T. Roscilde, Quantum Critical Metrology. *Phys. Rev. Lett.* **121**, 020402 (2018), <https://link.aps.org/doi/10.1103/PhysRevLett.121.020402>.
14. A. Niezgoda, J. Chwedeńczuk, Many-Body Nonlocality as a Resource for Quantum-Enhanced Metrology. *Phys. Rev. Lett.* **126**, 210506 (2021), <https://link.aps.org/doi/10.1103/PhysRevLett.126.210506>.
15. T. Comparin, F. Mezzacapo, M. Robert-de Saint-Vincent, T. Roscilde, Scalable Spin Squeezing from Spontaneous Breaking of a Continuous Symmetry. *Phys. Rev. Lett.* **129**, 113201 (2022), <https://link.aps.org/doi/10.1103/PhysRevLett.129.113201>.
16. G. Bornet, *et al.*, Scalable spin squeezing in a dipolar Rydberg atom array. *Nature* **621**, 728–733 (2023), <http://dx.doi.org/10.1038/s41586-023-06414-9>.
17. W. J. Eckner, *et al.*, Realizing spin squeezing with Rydberg interactions in an optical clock. *Nature* **621**, 734–739 (2023), <http://dx.doi.org/10.1038/s41586-023-06360-6>.
18. J. Franke, *et al.*, Quantum-enhanced sensing on optical transitions through finite-range interactions. *Nature* **621**, 740–745 (2023), <http://dx.doi.org/10.1038/s41586-023-06472-z>.
19. M. Block, *et al.*, Scalable spin squeezing from finite-temperature easy-plane magnetism. *Nat. Phys.* **20**, 1575–1581 (2024), <http://dx.doi.org/10.1038/s41567-024-02562-5>.
20. W. Wu, *et al.*, Spin squeezing in an ensemble of nitrogen–vacancy centres in diamond. *Nature* **646**, 74–80 (2025), <http://dx.doi.org/10.1038/s41586-025-09524-8>.

21. H. Gao, *et al.*, Signal amplification in a solid-state sensor through asymmetric many-body echo. *Nature* **646**, 68–73 (2025), <http://dx.doi.org/10.1038/s41586-025-09452-7>.
22. T. Guhr, A. Müller–Groeling, H. A. Weidenmüller, Random-matrix theories in quantum physics: Common concepts. *Phys. Rep.* **299**, 189–425 (1998), <https://www.sciencedirect.com/science/article/pii/S0370157397000884>.
23. S. L. Braunstein, C. M. Caves, Statistical distance and the geometry of quantum states. *Phys. Rev. Lett.* **72**, 3439–3443 (1994), <https://link.aps.org/doi/10.1103/PhysRevLett.72.3439>.
24. P. Hauke, M. Heyl, L. Tagliacozzo, P. Zoller, Measuring multipartite entanglement through dynamic susceptibilities. *Nat. Phys.* **12**, 778–782 (2016), <https://www.nature.com/articles/nphys3700>.
25. P. Zanardi, N. Paunković, Ground state overlap and quantum phase transitions. *Phys. Rev. E* **74**, 031123 (2006), <https://link.aps.org/doi/10.1103/PhysRevE.74.031123>.
26. M. Gärtner, P. Hauke, A. M. Rey, Relating Out-of-Time-Order Correlations to Entanglement via Multiple-Quantum Coherences. *Phys. Rev. Lett.* **120**, 040402 (2018), <https://link.aps.org/doi/10.1103/PhysRevLett.120.040402>.
27. J. Smith, *et al.*, Many-body localization in a quantum simulator with programmable random disorder. *Nat. Phys.* **12**, 907–911 (2016), <https://www.nature.com/articles/nphys3783>.
28. J.-Y. Desaulles, F. Pietracaprina, Z. Papić, J. Goold, S. Pappalardi, Extensive Multipartite Entanglement from $su(2)$ Quantum Many-Body Scars. *Phys. Rev. Lett.* **129**, 020601 (2022), <https://link.aps.org/doi/10.1103/PhysRevLett.129.020601>.
29. Y. Chu, X. Li, J. Cai, Quantum Delocalization on Correlation Landscape: The Key to Exponentially Fast Multipartite Entanglement Generation. *Phys. Rev. Lett.* **133**, 110201 (2024), <https://link.aps.org/doi/10.1103/PhysRevLett.133.110201>.
30. See Supplementary Materials for additional details of derivation and calculation .

31. M. Ledoux, *The Concentration of Measure Phenomenon* (American Mathematical Society) (2001), <http://dx.doi.org/10.1090/surv/089>.
32. G. W. Anderson, A. Guionnet, O. Zeitouni, *An Introduction to Random Matrices* (Cambridge University Press, Cambridge) (2009), <https://www.cambridge.org/core/books/an-introduction-to-random-matrices/8992DA8EB0386651E8DA8214A1FC7241>.
33. D. Bakry, I. Gentil, M. Ledoux, *Analysis and Geometry of Markov Diffusion Operators* (Springer International Publishing) (2014), <http://dx.doi.org/10.1007/978-3-319-00227-9>.
34. Y. Nakata, M. Muraio, Diagonal-unitary 2-design and their implementations by quantum circuits. *Int. J. Quantum Inf.* **11**, 1350062 (2013), <https://www.worldscientific.com/doi/abs/10.1142/S0219749913500627>.
35. B. S. Mityagin, The Zero Set of a Real Analytic Function. *Math. Notes* **107**, 529–530 (2020), <http://dx.doi.org/10.1134/S0001434620030189>.
36. S. Aaronson, Y. Atia, L. Susskind, On the Hardness of Detecting Macroscopic Superpositions. *arXiv:2009.07450* (2020), <https://arxiv.org/abs/2009.07450>.
37. B. Kobrin, *et al.*, A Universal Protocol for Quantum-Enhanced Sensing via Information Scrambling. *arXiv:2411.12794* (2024), <https://arxiv.org/abs/2411.12794>.
38. Y. Ge, *et al.*, Information-Scrambling-Enhanced Quantum Sensing Beyond the Standard Quantum Limit. *arXiv:2512.21157* (2025), <https://arxiv.org/abs/2512.21157>.
39. G. Hu, *et al.*, Quantum-Enhanced Sensing Enabled by Scrambling-Induced Genuine Multiparticle Entanglement. *arXiv:2601.22503* (2026), <https://arxiv.org/abs/2601.22503>.
40. L. Erdős, D. Schröder, Phase Transition in the Density of States of Quantum Spin Glasses. *Math. Phys. Anal. Geom.* **17**, 441–464 (2014), <http://dx.doi.org/10.1007/s11040-014-9164-3>.
41. J. Cotler, N. Hunter-Jones, J. Liu, B. Yoshida, Chaos, complexity, and random matrices. *J. High Energy Phys.* **2017**, 48 (2017), [https://doi.org/10.1007/JHEP11\(2017\)048](https://doi.org/10.1007/JHEP11(2017)048).

42. L. Hartmann, J. Calsamiglia, W. Dür, H. J. Briegel, Weighted graph states and applications to spin chains, lattices and gases. *J. Phys. B* **40**, S1–S44 (2007), <http://dx.doi.org/10.1088/0953-4075/40/9/S01>.
43. Y. Chu, X. Li, J. Cai, Strong Quantum Metrological Limit from Many-Body Physics. *Phys. Rev. Lett.* **130**, 170801 (2023), <https://link.aps.org/doi/10.1103/PhysRevLett.130.170801>.
44. S. Colombo, *et al.*, Time-reversal-based quantum metrology with many-body entangled states. *Nat. Phys.* **18**, 925–930 (2022), <https://www.nature.com/articles/s41567-022-01653-5>.
45. Q. Liu, *et al.*, Nonlinear interferometry beyond classical limit enabled by cyclic dynamics. *Nat. Phys.* **18**, 167–171 (2022), <https://www.nature.com/articles/s41567-021-01441-7>.
46. J. M. Chow, *et al.*, Simple All-Microwave Entangling Gate for Fixed-Frequency Superconducting Qubits. *Phys. Rev. Lett.* **107**, 080502 (2011), <https://link.aps.org/doi/10.1103/PhysRevLett.107.080502>.
47. S. Sheldon, E. Magesan, J. M. Chow, J. M. Gambetta, Procedure for systematically tuning up cross-talk in the cross-resonance gate. *Phys. Rev. A* **93**, 060302 (2016), <https://link.aps.org/doi/10.1103/PhysRevA.93.060302>.
48. F. Arute, *et al.*, Quantum supremacy using a programmable superconducting processor. *Nature* **574**, 505–510 (2019), <https://www.nature.com/articles/s41586-019-1666-5>.
49. T. I. Andersen, *et al.*, Thermalization and criticality on an analogue–digital quantum simulator. *Nature* **638**, 79–85 (2025), <http://dx.doi.org/10.1038/s41586-024-08460-3>.
50. X. H. H. Zhang, D. Malz, P. Rabl, Robust Superradiance and Spontaneous Spin Ordering in Disordered Waveguide QED. *arXiv:2510.13671* (2025), <https://arxiv.org/abs/2510.13671>.
51. P. Lodahl, S. Mahmoodian, S. Stobbe, Interfacing single photons and single quantum dots with photonic nanostructures. *Rev. Mod. Phys.* **87**, 347–400 (2015), <https://link.aps.org/doi/10.1103/RevModPhys.87.347>.

52. E. J. Davis, *et al.*, Probing many-body dynamics in a two-dimensional dipolar spin ensemble. *Nat. Phys.* **19**, 836–844 (2023), <http://dx.doi.org/10.1038/s41567-023-01944-5>.
53. M. Lei, *et al.*, Quantum thermalization and Floquet engineering in a spin ensemble with a clock transition. *Nat. Phys.* **21**, 1196–1202 (2025), <http://dx.doi.org/10.1038/s41567-025-02943-4>.
54. P. D. Gregory, *et al.*, Second-scale rotational coherence and dipolar interactions in a gas of ultracold polar molecules. *Nat. Phys.* **20**, 415–421 (2024), <http://dx.doi.org/10.1038/s41567-023-02328-5>.
55. O. Gühne, G. Tóth, Entanglement detection. *Phys. Rep.* **474**, 1–75 (2009), <http://dx.doi.org/10.1016/j.physrep.2009.02.004>.
56. D. Gross, S. T. Flammia, J. Eisert, Most Quantum States Are Too Entangled To Be Useful As Computational Resources. *Phys. Rev. Lett.* **102**, 190501 (2009), <https://link.aps.org/doi/10.1103/PhysRevLett.102.190501>.
57. M. J. Bremner, C. Mora, A. Winter, Are Random Pure States Useful for Quantum Computation? *Phys. Rev. Lett.* **102**, 190502 (2009), <https://link.aps.org/doi/10.1103/PhysRevLett.102.190502>.
58. M. Howard, J. Wallman, V. Veitch, J. Emerson, Contextuality supplies the ‘magic’ for quantum computation. *Nature* **510**, 351–355 (2014), <https://www.nature.com/articles/nature13460>.
59. F. G. S. L. Brandão, A. W. Harrow, M. Horodecki, Local random quantum circuits are approximate polynomial-designs. *Comm. Math. Phys.* **346**, 397–434 (2016), <https://doi.org/10.1007/s00220-016-2706-8>.
60. T. Schuster, J. Haferkamp, H.-Y. Huang, Random unitaries in extremely low depth. *Science* **389**, 92–96 (2025), <https://www.science.org/doi/10.1126/science.adv8590>.

Acknowledgments

This work was supported by the National Natural Science Foundation of China (12425414, U25D9006, 12174138, 12304572), Quantum Science and Technology-National Science and Technology Major Project (2024ZD0300900,2024ZD0300902), and the German Research Foundation (DFG) via project492547816 (TRR 360). Y.C. also acknowledges the support of the Fundamental Research Support Program of Huazhong University of Science and Technology (2025BRB001) and the Major Science and Technology Project of Hubei Province (2025BEA001). The authors declare no competing financial or non-financial interests.

Data Availability

The data that support the findings of this study are included in this article and are available from the corresponding author upon reasonable request.

Appendix

The introduced α -random unitary ensembles [see Eq. (2) in the main text] can generate metrologically useful states attaining Heisenberg-limited precision, rigorously supported by Theorem 1 and the concentration-of-measure phenomena in Theorem 2 as well as the two corollaries for two explicit class of ERSs. Below, we present the key ingredients underlying our main results, showing how engineered randomness serves as a promising approach for exploring the exponentially vast Hilbert space. We also detail the implementation of time-reversal quantum-enhanced metrology using engineered random states (ERSs) in a trapped-ion platform.

A. Proof of Theorem 1: average Heisenberg-limited scaling

In Heisenberg picture, for an arbitrary operator \mathcal{A} , the characteristic first-moment structure of α -random unitary ensembles in Eq. (2) yields Lemma 1,

$$\begin{aligned}\mathbb{E}_{U \sim \mathcal{U}_\alpha}[U^\dagger \mathcal{A} U] &= \sum_{i_1, i_2, j_1, j_2} \mathbb{E}_{U \sim \mathcal{U}_\alpha}[U_{i_1 j_1} U_{i_2, j_2}^*] \mathcal{A}_{i_2 i_1} |j_2\rangle \langle j_1| \\ &= \sum_{i_1, i_2, j_1, j_2} \alpha \delta_{i_1 j_1} \delta_{i_2 j_2} \mathcal{A}_{i_2 i_1} |j_2\rangle \langle j_1| + (1 - \alpha) \sum_{i_1 i_2 j_1 j_2} \Delta_{i_1, i_2, j_1, j_2} \mathcal{A}_{i_2 i_1} |j_2\rangle \langle j_1| \quad (15) \\ &= \alpha \mathcal{A} + (1 - \alpha) \frac{\text{tr}(\mathcal{A})}{D} \mathbb{I}.\end{aligned}$$

For convenience, we define a function over the high-dimensional space of U ,

$$f(U; \mathcal{A}) = \langle \Psi_U | \mathcal{A} | \Psi_U \rangle = \langle \Psi | U^\dagger \mathcal{A} U | \Psi \rangle, \quad (16)$$

which evaluates the expectation value of \mathcal{A} after the action of U on the initial state $|\Psi\rangle$. Averaging over the ensemble \mathcal{U}_α gives the simple identity

$$\mathbb{E}_{U \sim \mathcal{U}_\alpha}[f(U; \mathcal{A})] = \alpha \langle \Psi | \mathcal{A} | \Psi \rangle + (1 - \alpha) \frac{\text{tr}(\mathcal{A})}{D}. \quad (17)$$

This result allows the ensemble-averaged QFI in Eq. (1), associated with a traceless collective Hermitian generator $\mathcal{O} = \sum_{m=1}^N \mathcal{O}_m$, to be written as

$$\begin{aligned}\mathbb{E}_{U \sim \mathcal{U}_\alpha}[F_Q] &= 4\mathbb{E}_{U \sim \mathcal{U}_\alpha}[f(U; \mathcal{O}^2)] - \mathbb{E}_{U \sim \mathcal{U}_\alpha}[f^2(U; \mathcal{O})] \\ &= \alpha \langle \Psi | \mathcal{O}^2 | \Psi \rangle - \mathbb{E}_{U \sim \mathcal{U}_\alpha}[f^2(U; \mathcal{O})] + (1 - \alpha) \frac{\text{tr}(\mathcal{O}^2)}{D}.\end{aligned} \quad (18)$$

In high-dimensional spaces, the function $f(U; \mathcal{A})$ is often governed by the concentration-of-measure phenomenon, ensuring that $f(U; \mathcal{A})$ remains tightly clustered around its mean value in Eq. (17). By assuming that $\mathbb{E}_{U \sim \mathcal{U}_\alpha} [f^2(U; \mathcal{O})] - \mathbb{E}_{U \sim \mathcal{U}_\alpha}^2 [f(U; \mathcal{O})] \leq \Theta(N)$, the second term simplifies to the square of the mean, giving rise to

$$\mathbb{E}_{U \sim \mathcal{U}_\alpha} [F_Q] = \alpha \langle \Psi | \mathcal{O}^2 | \Psi \rangle - \alpha^2 \langle \Psi | \mathcal{O} | \Psi \rangle^2 + (1 - \alpha) \frac{\text{tr}(\mathcal{O}^2)}{D} + \Theta(N). \quad (19)$$

This compact form directly reproduces Theorem 1 where $\langle \Psi | \mathcal{O}^2 | \Psi \rangle = \langle \Psi | \mathcal{O} | \Psi \rangle^2 = \lambda^2 N^2$ and $\text{tr}(\mathcal{O}^2)/D = \Theta(N)$ holds.

B. Proof of Theorem 2: concentration of superior metrological usefulness

Starting from Eq. (7) in Theorem 2, we firstly evaluate the variance of the expectation value function $f(U, \mathcal{O})$ associated with the generator of parameter change. We define $y = f^2(U; \mathcal{O}) - \mathbb{E}_{U \sim \mathcal{U}_\alpha}^2 [f(U; \mathcal{O})]$. By using that $\mathbb{E}_{U \sim \mathcal{U}_\alpha} [f(U, \mathcal{O})] = \alpha \langle \Psi | \mathcal{O} | \Psi \rangle = \alpha \lambda N$, the probability of $|y| > \epsilon$ is upper bounded by

$$\begin{aligned} \Pr(|y| \geq \epsilon) &\leq \Pr\left(|f(U; \mathcal{O}) - \mathbb{E}_{U \sim \mathcal{U}_\alpha} [f(U; \mathcal{O})]| \geq \frac{\epsilon}{2\mathbb{E}_{U \sim \mathcal{U}_\alpha} [f(U; \mathcal{O})]}\right) \\ &\leq 2 \exp\left(-\frac{c\epsilon^2}{4\alpha^2 \lambda^2 N^2 L_{\mathcal{O}}^2}\right) = 2 \exp\left(-\Theta\left(\frac{D\epsilon^2}{\text{poly}(N)}\right)\right). \end{aligned} \quad (20)$$

This inequality strictly implies that the variance of $f(U, \mathcal{O})$, namely $\mathbb{E}_{U \sim \mathcal{U}_\alpha} [y]$, is exponentially small in the Hilbert space dimension. Next, we characterize the statistical behavior of the QFI by defining the following quantity,

$$\bar{F}_Q \equiv 4\mathbb{E}_{U \sim \mathcal{U}_\alpha} [f(U; \mathcal{O}^2)] - 4\mathbb{E}_{U \sim \mathcal{U}_\alpha}^2 [f(U; \mathcal{O})] = 4\alpha(1 - \alpha)\lambda^2 N^2 + \Theta(N). \quad (21)$$

We examine the concentration of the QFI around \bar{F}_Q by bounding the deviation probability,

$$\begin{aligned} \Pr(|F_Q - \bar{F}_Q| \geq \epsilon) &= \Pr\left(|4f(U; \mathcal{O}^2) - 4\mathbb{E}[f(U; \mathcal{O}^2)] - 4f^2(U; \mathcal{O}) + 4\mathbb{E}^2[f(U; \mathcal{O})]| \geq \epsilon\right) \\ &\leq \Pr\left(|f(U; \mathcal{O}^2) - \mathbb{E}[f(U; \mathcal{O}^2)]| + |f^2(U; \mathcal{O}) - \mathbb{E}^2[f(U; \mathcal{O})]| \geq \frac{\epsilon}{4}\right) \\ &\leq \Pr\left(|f(U; \mathcal{O}^2) - \mathbb{E}[f(U; \mathcal{O}^2)]| \geq \frac{\epsilon}{8}\right) + \Pr\left(|f^2(U; \mathcal{O}) - \mathbb{E}^2[f(U; \mathcal{O})]| \geq \frac{\epsilon}{8}\right) \\ &\leq 2 \exp\left(-\frac{c\epsilon^2}{64L_{\mathcal{O}^2}^2}\right) + 2 \exp\left(-\frac{c\epsilon^2}{256\alpha^2 \lambda^2 N^2 L_{\mathcal{O}}^2}\right) \\ &\leq \exp\left(-\Theta\left(\frac{D\epsilon^2}{\text{poly}(N)}\right)\right). \end{aligned} \quad (22)$$

By further making a replacement of $\epsilon \rightarrow \epsilon \bar{F}_Q$ in the above result and noticing that $\bar{F}_Q = \Theta(N^2)$, we find that

$$\Pr\left(|F_Q - \bar{F}_Q| \geq \epsilon \bar{F}_Q\right) \leq \exp\left(-\Theta\left(\frac{D\epsilon^2 \bar{F}_Q^2}{\text{poly}(N)}\right)\right) = \exp\left(-\Theta\left(\frac{D\epsilon^2}{\text{poly}(N)}\right)\right), \quad (23)$$

which directly yields Theorem 2 by taking ϵ to be a constant close to one.

C. RPS manifold: generation and concentration

Building on the condition in Eq. (10), the first moments of random diagonal unitaries exploited in the first construction of α -random unitary ensemble reads

$$\mathbb{E}[\Phi_{i_1 j_1} \Phi_{i_2 j_2}^*] = \begin{cases} \alpha \delta_{i_1 j_1} \delta_{i_2 j_2}, & \text{if } i_1 \neq i_2; \\ 1, & \text{if } i_1 = j_1 = i_2 = j_2. \end{cases} \quad (24)$$

In a N -qubit system, by following the same procedure as in Eq. (15), the operator contraction in Lemma 1 can be exactly derived for quantum operators $\mathcal{A} \in \{J_x, J_x^2\}$ under the special setting of $V = \mathbb{I}$ in Eq. (8). For an initial state fully polarized along the x axis, the above equation allows us to exactly express the ensemble-averaged QFI as

$$\mathbb{E}_{U \sim \mathcal{U}_\alpha} [F_Q] = \alpha(1 - \alpha)N^2 + (1 - \alpha)N, \quad (25)$$

where the second term originates from the fact that $\text{tr}(J_x^2)/D = N/4$.

Corollary 2.1—that most RPSs are metrologically useful—follows from the concentration-of-measure phenomenon in high-dimensional Gaussian spaces. Physically, this can be viewed as a manifestation of the law of large numbers: typical behavior dominates almost all realizations. Starting from RPS in Eq. (9), we introduce

$$f(\vec{\varphi}; \mathcal{A}) \equiv \langle \Psi(\varphi_1, \dots, \varphi_D) | \mathcal{A} | \Psi(\varphi_1, \dots, \varphi_D) \rangle = \frac{1}{D} \sum_{ab} \langle a | \mathcal{A} | b \rangle e^{i(\varphi_b - \varphi_a)}, \quad (26)$$

where $\vec{\varphi} = [\varphi_1, \dots, \varphi_D] \sim \mathcal{N}(0, \sigma^2 \mathbb{I}_D)$ is a Gaussian random vector with zero mean and covariance matrix $\sigma^2 \mathbb{I}_D$. We show in the Supplementary Materials that $f(\vec{\varphi}; \mathcal{O}) : \mathbb{R}^D \rightarrow \mathbb{R}$ is a Lipschitz continuous function with its Lipschitz constant bounded as

$$L = \sup_{\vec{\varphi} \in \mathbb{R}^D} \|\nabla f(\vec{\varphi}; \mathcal{A})\|_2 \leq \frac{N^\gamma}{\sqrt{D}}, \quad (27)$$

where $\gamma = 1$ for $\mathcal{A} = J_x$ and $\gamma = 2$ for $\mathcal{A} = J_x^2$, respectively. Based on the Gaussian concentration inequality, the probability that $f(\vec{\varphi}; \mathcal{A})$ deviates from its mean by more than ϵ is exponentially suppressed by the huge dimension of Hilbert space,

$$\Pr\left(\left|f(\vec{\varphi}; \mathcal{A}) - \mathbb{E}_{\vec{\varphi} \sim \mathcal{N}(0, \sigma^2 \mathbb{I}_D)}[f(\vec{\varphi}; \mathcal{A})]\right| \geq \epsilon\right) \leq 2 \exp\left(-\frac{D\epsilon^2}{2N^{2\gamma}\sigma^2}\right). \quad (28)$$

This result shows that $f(\vec{\varphi}; \mathcal{A})$ is overwhelmingly concentrated around its mean value, ensuring that almost all RPSs exhibit the typical metrological usefulness based on Theorem 2. That is, the probability of encountering a RPS that cannot achieve Heisenberg-limited scaling is exponentially suppressed in the Hilbert space dimension,

$$\Pr\left(F_Q(\vec{\varphi}; J_x) < \Theta(N^2)\right) \leq \exp\left[-\Theta\left(\frac{D}{\sigma^2}\right)\right], \quad (29)$$

where $F_Q(\vec{\varphi}; J_x)$ denotes the quantum Fisher information associated with the collective spin generator J_x .

D. CSS manifold: generation and concentration

A key simplification arises from the invariance of Haar measure under both left and right multiplication. By leveraging this property, the second construction of the α -random unitary ensemble takes the compact form

$$U = V\hat{\Phi}V^\dagger, \quad (30)$$

where V is a Haar-random unitary on $SU(D)$ and $\hat{\Phi}$ denotes the eigenvalue matrix of Φ . The first moments of U can then be evaluated as

$$\begin{aligned} \mathbb{E}[U_{i_1 j_1} U_{i_2 j_2}^*] &= \sum_{mn} \mathbb{E}\left[V_{i_1 m} V_{j_2 n} V_{j_1 m}^* V_{i_2 n}^*\right] \hat{\Phi}_{mm} \hat{\Phi}_{nn}^* \\ &= \frac{\alpha D^2 - 1}{D^2 - 1} \delta_{i_1 j_1} \delta_{i_2 j_2} + \frac{D}{D^2 - 1} (1 - \alpha) \delta_{i_1 i_2} \delta_{j_1 j_2}, \end{aligned} \quad (31)$$

with the ensemble parameter $\alpha = |\text{tr}(\Phi)|^2/D$, which coincides with the normalized spectral form factor of Φ . The second line follows directly from the Haar-average over four unitary matrix elements, a result that is by now standard in random matrix theory. Crucially, this compact expression is consistent with Eq. (2), and it yields an identical exact operator contraction as in Lemma 1.

Theorem 1 in the main text establishes that the optimal ensemble contraction factor, $\alpha = |\text{tr}(\Phi)|^2/D$, takes the value $1/2$, leading directly to $\mathbb{E}(f_Q) = N/4 + 1/2$ for the QFI density of CSS.

We now show how this condition can be realized in a generic N -particle quantum system. Consider each particle to be a spin- J object with local dimension of $d = 2J + 1$, and take $\Phi = e^{-iH}$ as a local perturbation, for instance,

$$H = \chi S_z^{(1)} \otimes \mathbb{I} \otimes \mathbb{I} \cdots \otimes \mathbb{I}, \quad (32)$$

where $S_z = \text{diag}[J, J - 1, \dots, -J]$. Under such an assumption, we obtain that

$$\alpha = \left(\frac{\sin \left[\left(J + \frac{1}{2} \right) \chi \right]}{d \sin \left(\frac{\chi}{2} \right)} \right)^2. \quad (33)$$

For qubit systems ($J = 1/2$), this reduces to $\alpha = [\cos(\chi/2)]^2$, implying that $\alpha = 1/2$ is achieved at $\chi = \pi/2$. For qutrit ($J = 1$), one finds $\alpha = [1 + 2 \cos(\chi)]^2/9$, yielding $\alpha = 1/2$ at $\chi \approx 55.9^\circ$. The fixed unitary Φ may also represent a collective rotation. As an illustrative example, we focus on the N -qubit system with $\Phi = e^{-i\chi J_z}$. In this case, the ensemble parameter becomes

$$\alpha = \frac{1}{D} \left| \sum_{m=0}^N C_N^m e^{i(m-\frac{N}{2})\chi} \right|^2 = \left[\cos \left(\frac{\chi}{2} \right) \right]^{\frac{N}{2}}, \quad (34)$$

which reaches its optimal value $\alpha = 1/2$ at $\chi = \sqrt{2 \log 2/N} \approx \sqrt{1.4/N}$.

To establish that most CSS generated by our second construction are metrologically useful, we exploit the concentration-of-measure technique (32). In the same way, we consider the function returning the expectation value of the operator \mathcal{A} with respect to $|\Psi_U\rangle$,

$$f(V; \mathcal{A}) = \langle \Psi_U | \mathcal{A} | \Psi_U \rangle = \langle \Psi | V \Phi^\dagger V^\dagger \mathcal{A} V \Phi V^\dagger | \Psi \rangle. \quad (35)$$

The function $f(V; \mathcal{A}) : \text{SU}(D) \rightarrow \mathbb{R}$ is Lipschitz continuous on the special unitary group with its Lipschitz norm bounded by $\|f\|_{\text{Lip}} \leq 4\|\mathcal{A}\|_\infty$ (30). By Lévy's lemma, for any $\epsilon > 0$,

$$\Pr (|f(V; \mathcal{A}) - \mathbb{E}_{\text{Haar}}[f(V; \mathcal{A})]| \geq \epsilon) \leq 2 \exp \left(-\frac{D\epsilon^2}{64\|\mathcal{A}\|_\infty^2} \right), \quad (36)$$

This inequality shows that, as the dimension D of the Hilbert space increases, the value of $f(V)$ for a Haar-random V is exponentially concentrated around its mean. Based on Theorem 2, the QFI of the CSS class associated with the collective generator $\mathcal{O} = \sum_{m=1}^N \mathcal{O}_m$ obeys the following concentration inequality,

$$\Pr \left(F_Q(|\Psi_U\rangle; \mathcal{O}) < \Theta(N^2) \right) \leq \exp(-\Theta(D)), \quad (37)$$

which immediately implies the Corollary 2.2 in the main text. Detailed proofs are presented in the Supplementary Materials.

E. Experimental verification of ERS-enhanced metrology

We performed our experiments on IonQ’s Forte-1 quantum processor, which utilizes trapped ions with all-to-all qubit connectivity and high-fidelity operations, see Table S1 in the Supplementary Materials for detailed information about the device. To generate the ERSs, we implemented the unitary $U = V e^{iH} V^\dagger$ on the initial state $|0\rangle^{\otimes N}$, where $V^\dagger = \exp(-i\pi J_y/2)$ serves as a global $\pi/2$ pulse preparing the system in the $|+\rangle^{\otimes N}$ basis. The entangling Hamiltonian H in Eq. (14) was realized through a sequence of pairwise controlled-phase gates, $CP_{1j} \equiv CP[4\phi_{1j}] = \text{diag}[1, 1, 1, e^{4i\phi_{1j}}]$ between the first qubit and qubits $j = 2$ to N . These unitaries were transpiled into the hardware-native GPI, GPI2, and ZZ gate set and executed for three distinct sets of random interaction weights, see Table S2 in the Supplementary Materials.

To characterize the metrological usefulness, we employed a time-reversal protocol where, following the ERS preparation, a collective phase ϑ was encoded via the rotation $e^{i\vartheta J_z}$. The accumulated phase information was then mapped onto the return probability by applying the inverse unitary U^\dagger , namely

$$P(\vartheta) = |\langle \mathbf{x} | e^{-iH} e^{-i\vartheta J_x} e^{iH} | \mathbf{x} \rangle|^2 = |\langle \mathbf{0} | U^\dagger e^{-i\vartheta J_z} U | \mathbf{0} \rangle|^2. \quad (38)$$

Data were acquired by scanning $\vartheta \in [0, 0.5]$ across 50 evenly spaced points, each averaged over 100 experimental shots. The resulting signal was fitted to a damped sinusoidal function

$$P(\vartheta) = A e^{-b\vartheta} \cos(c\vartheta + d) + B, \quad (39)$$

from which we estimate the value of ϑ from the regions where the fitted curve has a large slope. The phase measurement uncertainty due to the quantum projection noise associated with measuring $P(\vartheta)$ can be evaluated as

$$\delta\vartheta^2 = \frac{P(\vartheta)[1 - P(\vartheta)]}{|\partial_\vartheta P(\vartheta)|^2}, \quad (40)$$

which provides a direct lower bound on the QFI density of the experimentally generated ERSs via the quantum Cramér–Rao bound, i.e. $f_Q \geq \delta\vartheta^{-2}/N$, with the metrological gain over the SQL estimated in decibels as $20 \log_{10}(\delta\vartheta_{\text{SQL}}/\delta\vartheta) = 20 \log_{10}(\delta\vartheta^{-1} N^{-1/2})$ (45).

Supplementary Materials for Engineered Randomness for Ubiquitous Quantum-Enhanced Metrology in Exponential-Dimensional Manifolds

Yaoming Chu^{1,2}, Baiyi Yu^{3,4,1}, Hartmut Häffner^{3,4}
Markus Heyl^{5,6}, Nathan Goldman^{7,8,9}, Jianming Cai^{1,2}

Corresponding authors: jianmingcai@hust.edu.cn

¹ *Center for Intelligence and Quantum Science (CIQS), International Joint Laboratory on Quantum Sensing and Quantum Metrology, School of Physics, Huazhong University of Science and Technology, Wuhan 430074, China*

² *Hubei Key Laboratory of Gravitation and Quantum Physics, Institute for Quantum Science and Engineering, Huazhong University of Science and Technology, Wuhan 430074, China*

³ *Department of Physics, University of California, Berkeley, CA 94720, USA*

⁴ *Challenge Institute for Quantum Computation, University of California, Berkeley, CA 94720, USA*

⁵ *Theoretical Physics III, Center for Electronic Correlations and Magnetism, Institute of Physics, University of Augsburg, Universitätsstr. 12a, 86159 Augsburg, Germany*

⁶ *Centre for Advanced Analytics and Predictive Sciences (CAAPS), University of Augsburg, Universitätsstr. 12a, 86159 Augsburg, Germany*

⁷ *CENOLI, Université Libre de Bruxelles, CP 231, Campus Plaine, B-1050 Brussels, Belgium*

⁸ *International Solvay Institutes, 1050 Brussels, Belgium*

⁹ *Laboratoire Kastler Brossel, Collège de France, CNRS, ENS-Université PSL, Sorbonne Université, 11 Place Marcelin Berthelot, 75005 Paris, France*

Contents

1	Preliminary	2
1.1	Quantum Fisher information	2
1.2	Concentration-of-measure phenomenon	3
1.3	Uselessness of Haar-random states	6
2	Engineered random unitary ensembles	7
2.1	First-moment structure of engineered random unitaries	8
2.2	Average Heisenberg-limited scaling	8
2.3	Concentration of superior metrological usefulness	9
2.4	Minimal overlap with the symmetric space	10
3	Random phase states	10
3.1	Diagonal α -random unitary ensemble	10
3.2	Random phase states	11
3.3	Concentration of metrological usefulness of RPSs	12
3.4	Exponential dimensionality of RPS manifold	13

4	Chimera-superposition states	14
4.1	Haar-random construction of unitary ensemble	14
4.2	Optimal perturbative unitary	15
4.3	Chimera-superposition states	16
4.4	Concentration of metrological usefulness of CSSs	18
4.5	CSS generation by random quantum circuits	18
4.6	Extension to Gaussian unitary ensemble	19
5	Experimental verification of enhanced metrology using ERSs	22
5.1	RPSs with correlated random phases	22
5.2	Enhanced metrology with ERSs using trapped ions	24

1 Preliminary

1.1 Quantum Fisher information

The quantum Fisher information (QFI) is the central figure of merit in quantum metrology, setting the ultimate bound on the precision of parameter estimation. It extends the classical Fisher information to the quantum domain by incorporating the full statistical structure of quantum states and underpins a broad range of quantum-enhanced sensing protocols. Geometrically, the QFI coincides with the Fubini–Study metric on the projective Hilbert space, offering an operational measure of state distinguishability under infinitesimal parameter variations.

Consider a family of quantum states, ρ_ϑ , smoothly parametrized by an unknown parameter ϑ . The QFI, $F_Q[\rho_\vartheta]$, is defined through the symmetric logarithmic derivative (SLD) L_ϑ :

$$F_Q[\rho_\vartheta] = \text{Tr}(\rho_\vartheta L_\vartheta^2), \quad \partial_\vartheta \rho_\vartheta = \frac{1}{2}(\rho_\vartheta L_\vartheta + L_\vartheta \rho_\vartheta). \quad (1.1)$$

The celebrated quantum Cramér–Rao bound links $F_Q[\rho_\vartheta]$ to the variance of an arbitrary unbiased estimator $\hat{\vartheta}$ via the following inequality [1],

$$\text{Var}(\hat{\vartheta}) \geq \frac{1}{F_Q[\rho_\vartheta]}, \quad (1.2)$$

thereby establishing QFI as the fundamental benchmark for precision limits in quantum metrology. For a general mixed state with spectral decomposition

$$\rho_\theta = \sum_i p_i(\theta) |i(\theta)\rangle\langle i(\theta)|, \quad (1.3)$$

the QFI can be expressed as

$$F_Q[\rho_\vartheta] = \sum_i \frac{(\partial_\vartheta p_i)^2}{p_i} + 2 \sum_{i \neq j: p_i + p_j > 0} \frac{(p_i - p_j)^2}{p_i + p_j} |\langle i | \partial_\vartheta j \rangle|^2. \quad (1.4)$$

The first term of the right-hand side corresponds to the classical Fisher information of the eigenvalue distribution, while the second one encodes the quantum contribution arising from the parameter-dependence of the eigenvectors. For a pure state $|\Psi_\vartheta\rangle$, this reduces to the well-known expression

$$F_Q[|\Psi_\vartheta\rangle] = 4 \left(\langle \partial_\vartheta \Psi_\vartheta | \partial_\vartheta \Psi_\vartheta \rangle - |\langle \Psi_\vartheta | \partial_\vartheta \Psi_\vartheta \rangle|^2 \right). \quad (1.5)$$

Below, we focus on the standard metrological setting where ϑ is imprinted by a unitary family of $e^{-i\vartheta\mathcal{O}}\rho e^{i\vartheta\mathcal{O}}$ with a ϑ -independent Hermitian generator \mathcal{O} from the initial input state ρ . In such a setting, the QFI usually takes the following complicated structure,

$$F_Q[\rho; \mathcal{O}] = 2 \sum_{i,j: p_i+p_j>0} \frac{(p_i - p_j)^2}{p_i + p_j} |\langle i|\mathcal{O}|j\rangle|^2. \quad (1.6)$$

where $\{p_i, |i\rangle\}$ are the eigenpairs of ρ . When $\rho = |\Psi\rangle\langle\Psi|$ is pure, such an intricate expression is then simplified to Eq. (1) in the main text that can easily be computed or measured, namely

$$F_Q[|\Psi\rangle; \mathcal{O}] = 4 (\langle\Psi|\mathcal{O}^2|\Psi\rangle - \langle\Psi|\mathcal{O}|\Psi\rangle^2). \quad (1.7)$$

Over the past two decades, QFI has evolved from a foundational concept in quantum metrology into a versatile diagnostic tool across quantum information science. While serving as an effective witness of multipartite entanglement as a remarkable example [2, 3], it has also emerged as a probe of strongly correlated many-body systems, providing insights into quantum phase transitions [4], nonlocal correlations [5], multiple-quantum coherence [6], and nonergodic dynamics such as many-body localization [7] and quantum many-body scars [8].

1.2 Concentration-of-measure phenomenon

In this section, we outline a key ingredient underlying the technical results in the main text—the concentration-of-measure phenomenon [9, 10]. Informally, this concept asserts that a function of many independent random variables—provided it depends only weakly on each individual variable and is Lipschitz continuous—is overwhelmingly likely to be close to its mean. For our purpose, the following analysis will focus on Lipschitz concentration inequalities for the special unitary group $SU(D)$ and high-dimensional Gaussian measures. Both cases express the same core idea: Lipschitz functions over high-dimensional continuous spaces—whether compact Lie groups or Euclidean spaces equipped with Gaussian measures—exhibit sharp concentration around their mean, with deviation probabilities decaying rapidly in the relevant dimension.

Geometric structure of $SU(D)$. We begin with $SU(D)$, a compact Lie group with a natural Riemannian structure [11]. At any point $U \in SU(D)$, the tangent space of $SU(D)$ possesses a natural identification to its Lie algebra $\mathfrak{su}(D)$, which consists of $D^2 - 1$ traceless Hermitian matrices. That is, there exists a linear isomorphism $T_U SU(D) \cong \mathfrak{su}(D)$, explicitly given by the map:

$$\mathfrak{su}(D) \ni X \mapsto \hat{X} = \left. \frac{d}{d\varphi} \right|_{\varphi=0} \exp(-i\varphi X)U = -iXU \in T_U SU(D). \quad (1.8)$$

This isomorphism allows us to define a natural bi-invariant Riemannian metric on $SU(D)$ by making use of the normalized positive-definite Killing form on $\mathfrak{su}(D)$,

$$g_U(\hat{X}, \hat{Y}) = \text{tr}(XY). \quad (1.9)$$

We point out that, a locally equivalent metric can be induced from the direct embedding of $SU(D)$ into the space of all the linear operators acting on the Hilbert space, where the Hilbert–Schmidt inner product is used. This inner product is defined as

$$g_{\text{HS}}(\hat{X}, \hat{Y}) = \langle \hat{X}, \hat{Y} \rangle_{\text{HS}} = \text{tr}(\hat{X}^\dagger \hat{Y}), \quad (1.10)$$

which further induce the Hilbert–Schmidt norm (or Frobenius norm) for an operator as $\|\hat{X}\|_{\text{HS}} = \text{tr}(\hat{X}^\dagger \hat{X})$. With this embedding, the Riemannian metric at any point $U \in \text{SU}(D)$ coincides with the Hilbert–Schmidt metric,

$$g_U(\hat{X}, \hat{Y}) = g_{\text{HS}}(\hat{X}, \hat{Y}). \quad (1.11)$$

With the metric $g_U(\hat{X}, \hat{Y})$ in place, the geodesic connecting two elements $U, V \in \text{SU}(D)$ is

$$\gamma(t) = Ue^{tH} \quad \text{with } t \in [0, 1], \quad (1.12)$$

where $H = \log(U^\dagger V)$ and its length defines the geodesic distance between U and V ,

$$d_{\text{geo}}(U, V) = \int_\gamma \sqrt{g_{\text{HS}}\left(\frac{d\gamma}{dt}, \frac{d\gamma}{dt}\right)} dt = \|\log(U^\dagger V)\|_{\text{HS}} \quad (1.13)$$

It should be pointed out that the geodesic distance is, in general, no smaller than the Hilbert–Schmidt distance between U and V ,

$$d_{\text{geo}}(U, V) \geq d_{\text{HS}}(U, V) = \|U - V\|_{\text{HS}}. \quad (1.14)$$

Concentration-of-measure on $\text{SU}(D)$. Having established basic ideas of the geometric structure of $\text{SU}(D)$, we now turn to its probabilistic properties. A central object is the *Haar measure*, denoted by μ , the unique probability measure on $\text{SU}(D)$ invariant under both left and right group actions: for any measurable set $\mathcal{S} \subseteq \text{SU}(D)$ and any $U, V \in \text{SU}(D)$,

$$\mu(\mathcal{S}) = \mu(U\mathcal{S}) = \mu(\mathcal{S}V), \quad (1.15)$$

where $U\mathcal{S} = \{US : S \in \mathcal{S}\}$ and $\mathcal{S}V = \{SV : S \in \mathcal{S}\}$. This invariance ensures that averaging over $\text{SU}(D)$ with respect to μ is unbiased and independent of the choice of coordinates, making the Haar measure the natural notion of uniformity on the group. Given a real-valued function on the group,

$$f : \text{SU}(D) \rightarrow \mathbb{R}, \quad (1.16)$$

we denote its Haar average as

$$\mathbb{E}_\mu[f] = \int_{\text{SU}(D)} f(U) d\mu(U). \quad (1.17)$$

In high dimensions, many such functions exhibit a remarkable form of typicality: they are sharply concentrated around their mean. This phenomenon is formalized by concentration inequalities, which bound the probability that $f(U)$ deviates significantly from $\mathbb{E}_\mu[f]$.

A key notion in this context is the *Lipschitz norm* of f , defined with respect to the geodesic distance on $\text{SU}(D)$:

$$\|f\|_{\text{Lip}} = \sup_{U \neq V} \frac{|f(U) - f(V)|}{d_{\text{geo}}(U, V)}, \quad (1.18)$$

which quantifies the sensitivity of the function f to changes in its argument. Functions with bounded Lipschitz norm cannot vary too abruptly across the group manifold, a prerequisite for strong concentration behavior. A prototypical result is the generalized *Lévy’s lemma* [9], which states that for any Lipschitz function $f : \text{SU}(D) \rightarrow \mathbb{R}$ and any $\epsilon > 0$ [11],

$$\Pr(|f(U) - \mathbb{E}_\mu[f]| \geq \epsilon) \equiv \mu(\{U \in \text{SU}(D) : |f(U) - \mathbb{E}_\mu[f]| \geq \epsilon\}) \leq 2 \exp\left(-\frac{D\epsilon^2}{4\|f\|_{\text{Lip}}^2}\right). \quad (1.19)$$

This inequality implies that, as the dimension D grows, the value of $f(U)$ for a Haar-random U is overwhelmingly likely to be exponentially close to its mean.

In the main text, we leverage this property to characterize the typical behavior of Chimera-superposed states and to analyze statistical fluctuations of the QFI as a function of U in high-dimensional spaces (Corollary 2.2 in the main text). The key task is to derive the Lipschitz norm of $f(U)$. A function $f(U)$ is said to be L -Lipschitz continuous if

$$|f(U) - f(V)| \leq L d_{\text{geo}}(U, V), \quad (1.20)$$

for all $U, V \in \text{SU}(D)$, which directly implies $\|f\|_{\text{Lip}} \leq L$. When f is smooth, its Lipschitz norm admits the gradient representation

$$\|f\|_{\text{Lip}} = \sup_U \|\nabla f(U)\|_{\text{HS}}, \quad (1.21)$$

where the gradient $\nabla f(U)$ of the function f at the point U is defined through the condition

$$g_{\text{HS}}(\nabla f(U), \hat{X}) = \left. \frac{d}{d\varphi} \right|_{\varphi=0} f(\exp(-i\varphi X)U), \quad \forall X \in \mathfrak{su}(D). \quad (1.22)$$

A convenient criterion for bounding $\|f\|_{\text{Lip}}$ follows immediately: if

$$\left| \left. \frac{d}{d\varphi} \right|_{\varphi=0} f(\exp(-i\varphi X)U) \right| \leq C \|X\|_{\text{HS}}, \quad (1.23)$$

for all $U \in \text{SU}(D)$ and $X \in \mathfrak{su}(D)$, then it implies that $\|f\|_{\text{Lip}} \leq C$. As an illustrative example, we consider the expectation value function in Eq. (7) of Theorem 2 (see the main text) on $\text{SU}(D)$ as follows

$$f(U) = \langle \Psi | U^\dagger \mathcal{A} U | \Psi \rangle, \quad (1.24)$$

which compute the expectation value of the operator \mathcal{A} with respect to the rotated quantum state $|\Psi_U\rangle = U|\Psi\rangle$. The directional derivative of f along $X \in \mathfrak{su}(D)$ reads

$$\begin{aligned} \left| \left. \frac{d}{d\varphi} \right|_{\varphi=0} f(\exp(-i\varphi X)U) \right| &= \left| \langle \Psi | U^\dagger [\mathcal{A}, X] U | \Psi \rangle \right| \\ &\leq \|[\mathcal{A}, X]\|_\infty \leq 2\|\mathcal{A}\|_\infty \|X\|_\infty \leq 2\|\mathcal{A}\|_\infty \|X\|_{\text{HS}}, \end{aligned} \quad (1.25)$$

where $\|\bullet\|_\infty$ denotes the operator (or spectral) norm. This immediately yields the bound

$$\|f\|_{\text{Lip}} \leq 2\|\mathcal{A}\|_\infty. \quad (1.26)$$

We point out that this result can also be confirmed from the definition of Lipschitz continuity,

$$\begin{aligned} |f(U) - f(V)| &= \left| \langle \Psi | U^\dagger \mathcal{A} U - V^\dagger \mathcal{A} V | \Psi \rangle \right| \\ &\leq \left\| U^\dagger \mathcal{A} U - V^\dagger \mathcal{A} V \right\|_\infty \\ &= \left\| (U^\dagger - V^\dagger) \mathcal{A} U + V^\dagger \mathcal{A} (U - V) \right\|_\infty \\ &\leq 2\|\mathcal{A}\|_\infty \|U - V\|_\infty \\ &\leq 2\|\mathcal{A}\|_\infty \|U - V\|_{\text{HS}} \leq 2\|\mathcal{A}\|_\infty d_{\text{geo}}(U, V). \end{aligned} \quad (1.27)$$

Concentration of high-dimensional Gaussian measures. Next, we present the concentration inequality for Lipschitz functions defined on high-dimensional Gaussian spaces [9]. Let $f(\vec{x}) : \mathbb{R}^D \rightarrow \mathbb{R}$ be a L -Lipschitz continuous function, and let $\vec{x} \sim \mathcal{N}(0, \sigma^2 \mathbb{I}_D)$ be a Gaussian random vector with zero mean and covariance matrix $\sigma^2 \mathbb{I}_D$. Then, for all $\epsilon \geq 0$, the following inequality holds:

$$\Pr(|f(\vec{x}) - \mathbb{E}[f]| \geq \epsilon) \leq 2 \exp\left(-\frac{\epsilon^2}{2L^2\sigma^2}\right), \quad (1.28)$$

where L is the Lipschitz constant of $f(\vec{x})$. Specifically, it is defined with respect to the Euclidean norm on \mathbb{R}^D : for all $\vec{x}, \vec{y} \in \mathbb{R}^D$

$$|f(\vec{x}) - f(\vec{y})| \leq Ld(\vec{x}, \vec{y}) \quad \text{with} \quad d(\vec{x}, \vec{y}) \equiv \|\vec{x} - \vec{y}\|_2, \quad (1.29)$$

with $\|\bullet\|_2$ denotes the standard ℓ_2 norm. For a differentiable function $f(\vec{x})$, L can be estimated by computing the superior of its gradients, namely

$$L = \sup_{\vec{x} \in \mathbb{R}^D} \|\nabla f(\vec{x})\|_2. \quad (1.30)$$

Eq. (1.28) strictly highlight the phenomenon that Lipschitz functions evaluated on high-dimensional Gaussian inputs are overwhelmingly likely to take values close to their mean. Physically, this can be interpreted as a manifestation of the law of large numbers in high-dimensional spaces, where the ‘‘typical’’ behavior dominates the measure.

For example, high-dimensional Gaussian measures exhibit a striking geometric property: most of their probability mass is concentrated in a thin shell at a radius from the origin $r \sim \sigma\sqrt{D}$. This can be seen by considering the following length function,

$$f(\vec{x}) = \|\vec{x}\|_2 = \sqrt{\sum_{i=1}^D x_i^2}, \quad (1.31)$$

the Lipschitz constant of which can be easily obtained as $L = 1$. Consequently, the majority of the measure is confined to the thin annulus

$$\left\{ \vec{x} \in \mathbb{R}^D : \|\vec{x}\|_2 \in [\sigma\sqrt{D} - O(\sigma), \sigma\sqrt{D} + O(\sigma)] \right\}. \quad (1.32)$$

Indeed, $\|\vec{x}\|_2^2$ is distributed as $\sigma^2 \chi_D^2$, where χ_D^2 denotes the chi-squared distribution with D degrees of freedom. By the law of large numbers, as D increases, $\|\vec{x}\|_2^2/D \rightarrow \sigma^2$ with high probability, indicating that the vector length is sharply concentrated around $\sigma\sqrt{D}$. This geometric concentration underlies the exponential decay of the tail probability in the Gaussian concentration inequalities: Lipschitz functions cannot fluctuate significantly over this high-probability region, and the fraction of mass outside the typical shell is exponentially small in σ .

1.3 Uselessness of Haar-random states

In this section, we briefly examine the average metrological properties of generic many-body quantum states sampled uniformly from the Hilbert space [11]. Recall the well-known first-moment identities for the Haar measure over unitary matrices:

$$\mathbb{E}_{U \sim \text{Haar}}[U_{i_1 j_1} U_{i_2 j_2}^*] = \frac{1}{D} \delta_{i_1 i_2} \delta_{j_1 j_2}, \quad (1.33)$$

where $D = 2^N$ is the dimension of Hilbert space for an N -qubit system. From this, it immediately follows that the Haar average of an observable \mathcal{A} in the Heisenberg picture yields a fully depolarized operator,

$$\mathbb{E}_{U \sim \text{Haar}}[U^\dagger \mathcal{A} U] = \sum_{i_1 i_2 j_1 j_2} \mathbb{E}_{U \sim \text{Haar}}[U_{i_1 j_1} U_{i_2 j_2}^*] \mathcal{A}_{i_2 i_1} |j_2\rangle \langle j_1| = \frac{1}{D} \text{tr}(\mathcal{A}) \mathbb{I}. \quad (1.34)$$

Consequently, for traceless operators, their Haar average vanishes,

$$\mathbb{E}_{U \sim \text{Haar}}[U^\dagger \mathcal{A} U] = 0. \quad (1.35)$$

To assess metrological usefulness, we start from a fixed initial product state $|\Psi\rangle$, and define a Haar-random state by $|\Psi_U\rangle = U|\Psi\rangle$. The QFI of $|\Psi_U\rangle$ with respect to a Hermitian generator \mathcal{O} (e.g., a collective spin operator) of parameter change reads

$$F_Q[|\Psi_U\rangle, \mathcal{O}] = 4 (\langle \Psi_U | \mathcal{O}^2 | \Psi_U \rangle - \langle \Psi_U | \mathcal{O} | \Psi_U \rangle^2). \quad (1.36)$$

By using Eq. (1.34), one immediately finds that the average QFI over the Haar measure is given by

$$\mathbb{E}_{U \sim \text{Haar}}[F_Q] = \frac{4}{D} \text{tr}(\mathcal{O}^2) - 4 \mathbb{E}_{U \sim \text{Haar}}[\langle \Psi | U^\dagger \mathcal{O} U | \Psi \rangle^2]. \quad (1.37)$$

In order to evaluate the second term, we define

$$f(U; \mathcal{O}) = \langle \Psi | U^\dagger \mathcal{O} U | \Psi \rangle. \quad (1.38)$$

As established by Eq. (1.26), the Lipschitz norm of $f(U; \mathcal{O})$ with respect to the geodesic distance on $\text{SU}(D)$ satisfies

$$\|f\|_{\text{Lip}} \leq 2\|\mathcal{O}\|_\infty. \quad (1.39)$$

For collective observables in a N -qubit system, for example, $\mathcal{O} = J_\mu = \sum_{m=1}^N \sigma_\mu^{(m)}/2$ with $\mu = x, y, z$, one has $\|\mathcal{O}\|_\infty = N/2$, whereas the Hilbert space dimension grows exponentially, $D = 2^N$. Therefore, the Lipschitz constant is exponentially smaller than the effective dimension of Hilbert space, $\|f\|_{\text{Lip}} \ll \sqrt{D}$, which implies that $f(U; \mathcal{O})$ concentrates sharply around its mean value with exponentially suppressed statistical fluctuations. For a traceless Hermitian generator \mathcal{O} , the Haar average of $f(U; \mathcal{O})$ vanishes. As a result, one obtains that

$$\mathbb{E}[\langle \Psi | U^\dagger \mathcal{O} U | \Psi \rangle^2] \approx 0. \quad (1.40)$$

Hence, the average QFI simplifies to

$$\mathbb{E}[F_Q] \approx \frac{4}{D} \text{tr}(\mathcal{O}^2) = N. \quad (1.41)$$

This result clearly demonstrates that Haar-random states, despite being highly entangled, offer no quantum enhancement for metrology: their average QFI only scales linearly with the system size N , identical to that of product states. In a sense, this means that metrologically useful quantum states constitute a measure-zero subset in the Hilbert space, and a natural challenge occurs: *how can one identify the physically significant manifolds within the Hilbert space that yield a genuine quantum advantage?*

2 Engineered random unitary ensembles

In the main text, we propose a class of α -random unitary ensembles [see Eq. (2.1) in the main text] that can generate engineered random states (ERSs) attaining Heisenberg-limited precision, rigorously supported by Theorem 1 and the concentration-of-measure phenomena in Theorem 2. Below, we present the key ingredients underlying our main results, showing how engineered randomness serves as a promising approach for exploring the exponentially vast Hilbert space.

2.1 First-moment structure of engineered random unitaries

The unitaries sampled from an α -random unitary ensemble, \mathcal{U}_α , are characterized by the following first-moment identities

$$\mathbb{E}_{U \sim \mathcal{U}_\alpha} [U_{i_1 j_1} U_{i_2 j_2}^*] = \alpha \delta_{i_1 j_1} \delta_{i_2 j_2} + (1 - \alpha) \Delta_{i_1, i_2, j_1, j_2}. \quad (2.1)$$

By invoking the unitarity of U , namely

$$\sum_j U_{i_1 j} U_{i_2 j}^* = \delta_{i_1 i_2}, \quad \sum_i U_{i j_1} U_{i j_2}^* = \delta_{j_1 j_2}, \quad (2.2)$$

one immediately obtains that

$$\sum_j \Delta_{i_1, i_2, j, j} = \delta_{i_1 i_2}, \quad \sum_i \Delta_{i, i, j_1, j_2} = \delta_{j_1 j_2}. \quad (2.3)$$

In Heisenberg picture, for an arbitrary operator \mathcal{A} , the above first-moment identities lead to that

$$\begin{aligned} \mathbb{E}_{U \sim \mathcal{U}_\alpha} [U^\dagger \mathcal{A} U] &= \sum_{i_1, i_2, j_1, j_2} \mathbb{E}_{U \sim \mathcal{U}_\alpha} [U_{i_1 j_1} U_{i_2 j_2}^*] \mathcal{A}_{i_2 i_1} |j_2\rangle \langle j_1| \\ &= \alpha \mathcal{A} + (1 - \alpha) \sum_{i_1 i_2 j_1 j_2} \Delta_{i_1, i_2, j_1, j_2} \mathcal{A}_{i_2 i_1} |j_2\rangle \langle j_1|. \end{aligned} \quad (2.4)$$

To proceed, we assume that the second term acts as a completely depolarizing channel,

$$\mathcal{D}(\mathcal{A}) \equiv \sum_{i_1 i_2 j_1 j_2} \Delta_{i_1, i_2, j_1, j_2} \mathcal{A}_{i_2 i_1} |j_2\rangle \langle j_1| = c \frac{\mathbb{I}}{D}, \quad (2.5)$$

with c a real constant. By using Eq. (2.3), the trace of $\mathcal{D}(\mathcal{A})$ is exactly given by $\text{tr}(\mathcal{A})$. Consequently, the proportionality constant c equals $\text{tr}(\mathcal{A})$, yielding that

$$\mathcal{D}(\mathcal{A}) \equiv \sum_{i_1 i_2 j_1 j_2} \Delta_{i_1, i_2, j_1, j_2} \mathcal{A}_{i_2 i_1} |j_2\rangle \langle j_1| = \text{tr}(\mathcal{A}) \frac{\mathbb{I}}{D}. \quad (2.6)$$

2.2 Average Heisenberg-limited scaling

In Heisenberg picture, for an arbitrary operator \mathcal{A} , the characteristic first-moment structure of α -random unitary ensembles in Eq. (2.1) yields Lemma 1,

$$\begin{aligned} \mathbb{E}_{U \sim \mathcal{U}_\alpha} [U^\dagger \mathcal{A} U] &= \sum_{i_1, i_2, j_1, j_2} \mathbb{E}_{U \sim \mathcal{U}_\alpha} [U_{i_1 j_1} U_{i_2 j_2}^*] \mathcal{A}_{i_2 i_1} |j_2\rangle \langle j_1| \\ &= \sum_{i_1, i_2, j_1, j_2} \alpha \delta_{i_1 j_1} \delta_{i_2 j_2} \mathcal{A}_{i_2 i_1} |j_2\rangle \langle j_1| + (1 - \alpha) \sum_{i_1 i_2 j_1 j_2} \Delta_{i_1, i_2, j_1, j_2} \mathcal{A}_{i_2 i_1} |j_2\rangle \langle j_1| \\ &= \alpha \mathcal{A} + (1 - \alpha) \frac{\text{tr}(\mathcal{A})}{D} \mathbb{I}. \end{aligned} \quad (2.7)$$

For convenience, we define a function over the high-dimensional space of U ,

$$f(U; \mathcal{A}) = \langle \Psi_U | \mathcal{A} | \Psi_U \rangle = \langle \Psi | U^\dagger \mathcal{A} U | \Psi \rangle, \quad (2.8)$$

which evaluates the expectation value of \mathcal{A} after the action of U on the initial state $|\Psi\rangle$. Averaging over the ensemble \mathcal{U}_α gives the simple identity

$$\mathbb{E}_{U \sim \mathcal{U}_\alpha}[f(U; \mathcal{A})] = \alpha \langle \Psi | \mathcal{A} | \Psi \rangle + (1 - \alpha) \frac{\text{tr}(\mathcal{A})}{D}. \quad (2.9)$$

This result allows the ensemble-averaged QFI of $|\Psi_U\rangle$, associated with a traceless collective Hermitian generator $\mathcal{O} = \sum_{m=1}^N \mathcal{O}_m$ [see Eq. (1.7)], to be written as

$$\begin{aligned} \mathbb{E}_{U \sim \mathcal{U}_\alpha}[F_Q] &= 4\mathbb{E}_{U \sim \mathcal{U}_\alpha}[f(U; \mathcal{O}^2)] - \mathbb{E}_{U \sim \mathcal{U}_\alpha}[f^2(U; \mathcal{O})] \\ &= \alpha \langle \Psi | \mathcal{O}^2 | \Psi \rangle - \mathbb{E}_{U \sim \mathcal{U}_\alpha}[f^2(U; \mathcal{O})] + (1 - \alpha) \frac{\text{tr}(\mathcal{O}^2)}{D}. \end{aligned} \quad (2.10)$$

In high-dimensional spaces, the function $f(U; \mathcal{A})$ is often governed by the concentration-of-measure phenomenon, ensuring that $f(U; \mathcal{A})$ remains tightly clustered around its mean value in Eq. (2.9). By assuming that $\mathbb{E}_{U \sim \mathcal{U}_\alpha}[f(U; \mathcal{O})^2] - \mathbb{E}_{U \sim \mathcal{U}_\alpha}^2[f(U; \mathcal{O})] \leq \Theta(N)$, the second term simplifies to the square of the mean, giving rise to

$$\mathbb{E}_{U \sim \mathcal{U}_\alpha}[F_Q] = \alpha \langle \Psi | \mathcal{O}^2 | \Psi \rangle - \alpha^2 \langle \Psi | \mathcal{O} | \Psi \rangle^2 + (1 - \alpha) \frac{\text{tr}(\mathcal{O}^2)}{D} + \Theta(N). \quad (2.11)$$

This compact form directly reproduces Theorem 1 where $\langle \Psi | \mathcal{O}^2 | \Psi \rangle = \langle \Psi | \mathcal{O} | \Psi \rangle^2 = \lambda^2 N^2$ and $\text{tr}(\mathcal{O}^2)/D = \Theta(N)$ holds.

2.3 Concentration of superior metrological usefulness

Starting from Eq. (7) in Theorem 2 of the main text, we firstly evaluate the variance of the expectation value function $f(U, \mathcal{O})$ associated with the generator of parameter change. We define $y = f^2(U; \mathcal{O}) - \mathbb{E}_{U \sim \mathcal{U}_\alpha}^2[f(U; \mathcal{O})]$. By using that $\mathbb{E}_{U \sim \mathcal{U}_\alpha}[f(U, \mathcal{O})] = \alpha \langle \Psi | \mathcal{O} | \Psi \rangle = \alpha \lambda N$, the probability of $|y| > \epsilon$ is upper bounded by

$$\begin{aligned} \Pr(|y| \geq \epsilon) &\leq \Pr\left(|f(U; \mathcal{O}) - \mathbb{E}_{U \sim \mathcal{U}_\alpha}[f(U; \mathcal{O})]| \geq \frac{\epsilon}{2\mathbb{E}_{U \sim \mathcal{U}_\alpha}[f(U; \mathcal{O})]}\right) \\ &\leq 2 \exp\left(-\frac{c\epsilon^2}{4\alpha^2\lambda^2N^2L_{\mathcal{O}}^2}\right) = 2 \exp\left(-\Theta\left(\frac{D\epsilon^2}{\text{poly}(N)}\right)\right). \end{aligned} \quad (2.12)$$

This inequality strictly implies that the variance of $f(U, \mathcal{O})$, namely $\mathbb{E}_{U \sim \mathcal{U}_\alpha}[y]$, is exponentially small in the Hilbert space dimension. Next, we characterize the statistical behavior of the QFI by defining the following quantity,

$$\bar{F}_Q \equiv 4\mathbb{E}_{U \sim \mathcal{U}_\alpha}[f(U; \mathcal{O}^2)] - 4\mathbb{E}_{U \sim \mathcal{U}_\alpha}^2[f(U; \mathcal{O})] = 4\alpha(1 - \alpha)\lambda^2N^2 + \Theta(N). \quad (2.13)$$

We examine the concentration of the QFI around \bar{F}_Q by bounding the deviation probability,

$$\begin{aligned} \Pr(|F_Q - \bar{F}_Q| \geq \epsilon) &= \Pr(|4f(U; \mathcal{O}^2) - 4\mathbb{E}[f(U; \mathcal{O}^2)] - 4f^2(U; \mathcal{O}) + 4\mathbb{E}^2[f(U; \mathcal{O})]| \geq \epsilon) \\ &\leq \Pr\left(|f(U; \mathcal{O}^2) - \mathbb{E}[f(U; \mathcal{O}^2)]| + |f^2(U; \mathcal{O}) - \mathbb{E}^2[f(U; \mathcal{O})]| \geq \frac{\epsilon}{4}\right) \\ &\leq \Pr\left(|f(U; \mathcal{O}^2) - \mathbb{E}[f(U; \mathcal{O}^2)]| \geq \frac{\epsilon}{8}\right) + \Pr\left(|f^2(U; \mathcal{O}) - \mathbb{E}^2[f(U; \mathcal{O})]| \geq \frac{\epsilon}{8}\right) \\ &\leq 2 \exp\left(-\frac{c\epsilon^2}{64L_{\mathcal{O}^2}^2}\right) + 2 \exp\left(-\frac{c\epsilon^2}{256\alpha^2\lambda^2N^2L_{\mathcal{O}}^2}\right) \\ &\leq \exp\left(-\Theta\left(\frac{D\epsilon^2}{\text{poly}(N)}\right)\right). \end{aligned} \quad (2.14)$$

By further making a replacement of $\epsilon \rightarrow \epsilon \bar{F}_Q$ in the above result and noticing that $\bar{F}_Q = \Theta(N^2)$, we find that

$$\Pr\left(|F_Q - \bar{F}_Q| \geq \epsilon \bar{F}_Q\right) \leq \exp\left(-\Theta\left(\frac{D\epsilon^2 \bar{F}_Q^2}{\text{poly}(N)}\right)\right) = \exp\left(-\Theta\left(\frac{D\epsilon^2}{\text{poly}(N)}\right)\right), \quad (2.15)$$

which directly yields Theorem 2 by taking ϵ to be a constant close to one.

2.4 Minimal overlap with the symmetric space

Generally, the ERSs generated by an α -unitary ensemble \mathcal{U}_α reside deep within the full Hilbert space, far from the symmetric $O(N)$ -dimensional manifold. For concreteness, we focus on an N -qubit system. Its symmetric subspace is spanned by the Dicke basis $\{|D_N^k\rangle\}$ with $k = 0, 1, \dots, N$, with the associated projection operator

$$\mathbb{P} = \sum_{k=0}^N |D_N^k\rangle\langle D_N^k|. \quad (2.16)$$

Given an ERS, $|\Psi_U\rangle = U|\Psi\rangle$ with $U \in \mathcal{U}_\alpha$, its overlap with the symmetric subspace is quantified by the fidelity

$$\mathcal{F} = \text{tr}\left(\mathbb{P}|\Psi_U\rangle\langle\Psi_U|\right) = \text{tr}\left(U^\dagger\mathbb{P}U|\Psi\rangle\langle\Psi|\right) = \langle\Psi|U^\dagger\mathbb{P}U|\Psi\rangle \quad (2.17)$$

Averaging over \mathcal{U}_α yields

$$\mathbb{E}_{U \sim \mathcal{U}_\alpha}[\mathcal{F}] = \alpha \langle\Psi|\mathbb{P}|\Psi\rangle + \frac{1-\alpha}{D} \text{tr}(\mathbb{P}) \approx \alpha \langle\Psi|\mathbb{P}|\Psi\rangle, \quad (2.18)$$

where the second term is negligible, i.e. $\text{tr}(\mathbb{P}) = N + 1 \ll D = 2^N$. If the initial state is chosen as a fully polarized state along the z axis, namely $|\Psi\rangle = |0\rangle^{\otimes N}$, we immediately find $\mathbb{E}[\mathcal{F}] = \alpha$. Moreover, when starting from an initial state with no significant symmetric component, the overlap can be minimized even to zero, for example

$$|\Psi\rangle = |\uparrow\downarrow\downarrow \dots \downarrow\rangle \quad \text{or} \quad |\Psi\rangle = \frac{|\uparrow\downarrow\rangle - |\downarrow\uparrow\rangle}{\sqrt{2}} \otimes |\downarrow \dots \downarrow\rangle. \quad (2.19)$$

3 Random phase states

3.1 Diagonal α -random unitary ensemble

In the main text, our first example of an α -random unitary ensemble is to utilize random diagonal unitary matrices in the computational basis $\{|b\rangle\}_{b=1}^D$ conjugated by a fixed unitary operator, i.e. $U = V\Phi V^\dagger$ with $\Phi = \text{diag}[e^{i\varphi_1}, \dots, e^{i\varphi_D}]$. The random phases $\{\varphi_b\}_{b=1}^D$ obey independent identical probability distribution. Without loss of generality, we focus on a D -dimensional zero-mean normal distribution, denoted by $\mathcal{N}(0, \sigma^2 \mathbb{I}_D)$. Consequently, the first moments of Φ are given by

$$\mathbb{E}_{\vec{\varphi} \sim \mathcal{N}(0, \sigma^2 \mathbb{I}_D)}[\Phi_{i_1 j_1} \Phi_{i_2 j_2}^*] = \begin{cases} \alpha \delta_{i_1 j_1} \delta_{i_2 j_2} & \text{if } i_1 \neq i_2 \\ 1 & \text{if } i_1 = j_1 = i_2 = j_2 \end{cases} \quad (3.1)$$

with $\alpha = \exp(-\sigma^2)$. Under these assumptions, the first moments of U can be derived as

$$\mathbb{E}_{U \sim \mathcal{U}_\alpha}[U_{i_1 j_1} U_{i_2 j_2}^*] = \alpha \delta_{i_1 j_1} \delta_{i_2 j_2} + (1 - \alpha) \Delta_{i_1, i_2, j_1, j_2}, \quad (3.2)$$

where the second term of the right-hand side depends on the matrix elements of V ,

$$\Delta_{i_1, i_2, j_1, j_2} = \sum_b V_{i_1 b} V_{i_2 b}^* V_{j_1 b}^* V_{j_2 b}. \quad (3.3)$$

It satisfies the conditions that $\sum_j \Delta_{i_1, i_2, j, j} = \delta_{i_1 i_2}$ and $\sum_i \Delta_{i, i, j_1, j_2} = \delta_{j_1 j_2}$. In Heisenberg picture, for a quantum operator \mathcal{A} , the above first moments of U in Eq. (3.2) leads to that

$$\mathbb{E}_{U \sim \mathcal{U}_\alpha} [U^\dagger \mathcal{A} U] = \alpha \mathcal{A} + (1 - \alpha) \sum_b \sum_{j_1 j_2} (V^\dagger \mathcal{A} V)_{bb} V_{j_1 b}^* V_{j_2 b} |j_2\rangle \langle j_1|. \quad (3.4)$$

Next, we restrict our attention to a N -qubit system and set $\mathcal{A} = J_z$. As a result, the choice of $V = \exp(i\pi J_y/2)$ yields that $V^\dagger J_z V = J_x$, which has no diagonal elements in the computational basis: $(V^\dagger J_z V)_{bb} \equiv \langle b | V^\dagger J_z V | b \rangle = \langle b | J_x | b \rangle = 0$. In such a case, Eq. (3.4) is simplified as

$$\mathbb{E}_{U \sim \mathcal{U}_\alpha} [U^\dagger J_z U] = \alpha J_z. \quad (3.5)$$

Moreover, we have $(V^\dagger J_z^2 V)_{bb} \equiv \langle b | V^\dagger J_z^2 V | b \rangle = \langle b | J_x^2 | b \rangle$ for $\mathcal{A} = J_z^2$, which can be evaluated by decomposing J_x into the summation of local Pauli operators,

$$\langle b | V^\dagger J_z^2 V | b \rangle = \langle b | J_x^2 | b \rangle = \frac{1}{4} \sum_{m, n=1}^N \langle b | \sigma_x^{(m)} \sigma_x^{(n)} | b \rangle = \frac{N}{4}. \quad (3.6)$$

Substituting it into Eq. (3.4), we obtain that

$$\begin{aligned} \mathbb{E}_{U \sim \mathcal{U}_\alpha} [U^\dagger J_z^2 U] &= \alpha J_z^2 + (1 - \alpha) \frac{N}{4} \sum_{j_1 j_2} (V V^\dagger)_{j_2 j_1} |j_2\rangle \langle j_1| \\ &= \alpha J_z^2 + (1 - \alpha) \frac{N}{4} \sum_{j_1 j_2} \delta_{j_2 j_1} |j_2\rangle \langle j_1| \\ &= \alpha J_z^2 + (1 - \alpha) \frac{N}{4} \mathbb{I}. \end{aligned} \quad (3.7)$$

Note that Eqs. (3.5) and (3.7) straightforwardly correspond to the cases where $\mathcal{A} \in \{J_x, J_x^2\}$ and $V = \mathbb{I}$ in the main text. We refer to such a class of random unitaries as the *diagonal α -random unitary ensemble*, which satisfies Lemma 1 and subsequently Theorem 1 of the main text.

3.2 Random phase states

We continue to investigate the ERSs generated by the above diagonal α -random unitary ensemble in a N -qubit system with $D = 2^N$,

$$|\Psi_U\rangle = U|\Psi\rangle = V\Phi V^\dagger|\Psi\rangle. \quad (3.8)$$

For simplicity, we set the initial state as a fully polarized state along the x axis, i.e. $|\Psi\rangle = |+\rangle^{\otimes N}$, and $V = \mathbb{I}$, resulting in a generated ERS as follows,

$$|\Psi_U\rangle = \frac{1}{\sqrt{D}} \sum_{b=1}^D e^{i\varphi_b} |b\rangle, \quad (3.9)$$

which represents a class of *random phase states* (RPSs) [see Eq. (9) in the main text]. We note that the initial state can also be set as a non-symmetric one, e.g. $|\Psi\rangle = \exp(-i\pi J_y/2)|1\rangle \otimes |0\rangle^{\otimes(N-1)}$, the associated RPS then reads

$$|\Psi_U\rangle = \frac{1}{\sqrt{D}} \sum_{b=1}^D (-1)^{b_1} e^{i\varphi_b} |b\rangle. \quad (3.10)$$

Hereafter, we focus on the RPS defined in Eq. (3.9). The random phases $\{\varphi_b\}_{b=1}^D$ are independently sampled from distributions that satisfy $\mathbb{E}_{\varphi_b}[e^{\pm i\varphi_b}] = e^{-\sigma^2/2}$, which implies that

$$\mathbb{E}_{\vec{\varphi} \sim \mathcal{N}(0, \sigma^2 \mathbb{I}_D)}[e^{i(\varphi_a - \varphi_b)}] = \begin{cases} \alpha = e^{-\sigma^2} & \text{if } a \neq b, \\ 1 & \text{if } a = b. \end{cases} \quad (3.11)$$

In Schrödinger picture, the operator contraction effect can also be uncovered by considering the average expectation values,

$$\begin{aligned} \mathbb{E}_{U \sim \mathcal{U}_\alpha}[\langle \Psi_U | J_x | \Psi_U \rangle] &= \frac{1}{D} \sum_{ab} \langle b | J_x | a \rangle \mathbb{E}_{\vec{\varphi} \sim \mathcal{N}(0, \sigma^2 \mathbb{I}_D)}[e^{i(\varphi_a - \varphi_b)}] \\ &= \frac{\alpha}{D} \sum_{a \neq b} \langle b | J_x | a \rangle = \frac{\alpha}{D} \sum_{ab} \langle b | J_x | a \rangle = \alpha \langle \Psi | J_x | \Psi \rangle = \frac{\alpha N}{2}, \end{aligned} \quad (3.12)$$

and

$$\begin{aligned} \mathbb{E}_{U \sim \mathcal{U}_\alpha}[\langle \Psi_U | J_x^2 | \Psi_U \rangle] &= \frac{1}{D} \sum_{ab} \langle b | J_x^2 | a \rangle \mathbb{E}_{\vec{\varphi} \sim \mathcal{N}(0, \sigma^2 \mathbb{I}_D)}[e^{i(\varphi_a - \varphi_b)}] \\ &= \frac{\alpha}{D} \sum_{ab} \langle b | J_x^2 | a \rangle + \frac{1-\alpha}{D} \sum_a \langle a | J_x^2 | a \rangle = \alpha \langle \Psi | J_x^2 | \Psi \rangle + \frac{(1-\alpha)N}{4} \\ &= \alpha \frac{N^2}{4} + (1-\alpha) \frac{N}{4}. \end{aligned} \quad (3.13)$$

These results lead to that the average QFI associated with the collective spin generator J_x can be approximated as

$$\begin{aligned} \mathbb{E}_{U \sim \mathcal{U}_\alpha}[F_Q] &\approx \bar{F}_Q \equiv 4\mathbb{E}_{U \sim \mathcal{U}_\alpha}[\langle \Psi_U | J_x^2 | \Psi_U \rangle] - 4\left(\mathbb{E}_{U \sim \mathcal{U}_\alpha}[\langle \Psi_U | J_x | \Psi_U \rangle]\right)^2 \\ &= \alpha(1-\alpha)N^2 + (1-\alpha)N + O(N), \end{aligned} \quad (3.14)$$

provided that the function $f(U; J_x) \equiv \langle \Psi_U | J_x | \Psi_U \rangle$ versus U concentrates sharply around its mean, which we shall strictly prove in the following section. Hence, the average QFI of the RPSs in Eq. (3.9) scales quadratically with the system size N and is maximized at $\alpha = 1/2$ for large system sizes.

3.3 Concentration of metrological usefulness of RPSs

Corollary 2.1 in the main text—that most RPSs are metrologically useful—follows from the concentration-of-measure phenomenon in high-dimensional Gaussian spaces. Physically, this can be viewed as a manifestation of the law of large numbers: typical behavior dominates almost all realizations. Starting from RPS in Eq. (3.9), we introduce

$$f(\vec{\varphi}; \mathcal{A}) \equiv \langle \Psi(\varphi_1, \dots, \varphi_D) | \mathcal{A} | \Psi(\varphi_1, \dots, \varphi_D) \rangle = \frac{1}{D} \sum_{ab} \langle a | \mathcal{A} | b \rangle e^{i(\varphi_b - \varphi_a)}, \quad (3.15)$$

where $\vec{\varphi} = [\varphi_1, \dots, \varphi_D] \sim \mathcal{N}(0, \sigma^2 \mathbb{I}_D)$ is a Gaussian random vector with zero mean and covariance matrix $\sigma^2 \mathbb{I}_D$. We firstly show that $f(\vec{\varphi}; \mathcal{A}) : \mathbb{R}^D \rightarrow \mathbb{R}$ is a Lipschitz continuous function. Consider its derivative versus the k -th random phase,

$$\frac{\partial f}{\partial \varphi_k} = \frac{i}{D} \sum_{a \neq k} \langle a | \mathcal{A} | k \rangle e^{i(\varphi_k - \varphi_a)} - \frac{i}{D} \sum_{b \neq k} \langle k | \mathcal{A} | b \rangle e^{i(\varphi_b - \varphi_k)}. \quad (3.16)$$

Based on the triangle inequality, the magnitude is upper bounded by

$$\left| \frac{\partial f}{\partial \varphi_k} \right| = \frac{2}{D} \sum_{a \neq k} |\langle a | \mathcal{A} | k \rangle| \leq \frac{N^\gamma}{D}, \quad (3.17)$$

for $\mathcal{A} \in \{J_x, J_x^2\}$ with $\gamma = 1$ and 2 , respectively. Consequently, the Lipschitz constant of $f(\vec{\varphi}; \mathcal{A})$ is given by,

$$L_{\mathcal{A}} = \sup_{\vec{\varphi} \in \mathbb{R}^D} \|\nabla f(\vec{\varphi}; \mathcal{A})\|_2 = \sup_{\vec{\varphi} \in \mathbb{R}^D} \sqrt{\sum_{k=1}^D \left| \frac{\partial f}{\partial \varphi_k} \right|^2} \leq \sqrt{D \left(\frac{N^\gamma}{D} \right)^2} = \frac{N^\gamma}{D^{1/2}}. \quad (3.18)$$

Based on the Gaussian concentration inequality, the probability that $f(\vec{\varphi}; \mathcal{A})$ deviates from its mean by more than ϵ is exponentially suppressed by the huge dimension of Hilbert space,

$$\Pr\left(\left| f(\vec{\varphi}; \mathcal{A}) - \mathbb{E}_{\vec{\varphi} \sim \mathcal{N}(0, \sigma^2 \mathbb{I}_D)} [f(\vec{\varphi}; \mathcal{A})] \right| \geq \epsilon \right) \leq 2 \exp\left(-\frac{D\epsilon^2}{2N^{2\gamma}\sigma^2} \right). \quad (3.19)$$

This result shows that $f(\vec{\varphi}; \mathcal{A})$ is overwhelmingly concentrated around its mean value, ensuring that almost all RPSs exhibit the typical metrological usefulness based on Theorem 2 in the main text. That is, the probability of encountering a RPS that cannot achieve HL precision scaling is exponentially suppressed in the Hilbert space dimension,

$$\Pr\left(F_Q(\vec{\varphi}; J_x) < \Theta(N^2) \right) \leq \exp\left[-\Theta\left(\frac{D}{\sigma^2} \right) \right], \quad (3.20)$$

where $F_Q(\vec{\varphi}; J_x)$ denotes the QFI associated with the collective spin generator J_x .

3.4 Exponential dimensionality of RPS manifold

The manifold encompassing the RPSs defined in Eq. (3.9) possesses an exponential dimensionality; that is, its embedding dimension grows as $D = 2^N$. Here, the embedding dimension is defined as the dimension of the minimal linear subspace \mathcal{H}_{\min} such that all the possible RPS realizations $|\Psi_U\rangle \in \mathcal{H}_{\min}$. To establish this, we demonstrate that a set of D linearly independent vectors can be systematically constructed within the RPS manifold. For clarity, consider the case $D = 2$: given an initial RPS vector, a second linearly independent vector is almost surely obtained, owing to the independent distribution of the random phases $\{\varphi_b\}_{b=1}^D$. This logic extends naturally through induction. Suppose that for a given $D = n$ in Eq. (3.9), there exist n linearly independent vectors, namely

$$\begin{aligned} |\Psi_n^{(1)}\rangle &= \frac{1}{\sqrt{n}} \left(e^{i\varphi_1^{(1)}} |1\rangle + \dots + e^{i\varphi_n^{(1)}} |n\rangle \right), \\ &\dots \\ |\Psi_n^{(n)}\rangle &= \frac{1}{\sqrt{n}} \left(e^{i\varphi_1^{(n)}} |1\rangle + \dots + e^{i\varphi_n^{(n)}} |n\rangle \right). \end{aligned} \quad (3.21)$$

For the inductive step $D = n + 1$, we construct $n + 1$ RPS vectors as follows

$$\begin{aligned} |\Psi_{n+1}^{(1)}\rangle &= \frac{1}{\sqrt{n+1}} \left(\sqrt{n} |\Psi_n^{(1)}\rangle + e^{i\varphi_{n+1}^{(1)}} |n+1\rangle \right), \\ &\dots \\ |\Psi_{n+1}^{(n)}\rangle &= \frac{1}{\sqrt{n+1}} \left(\sqrt{n} |\Psi_n^{(n)}\rangle + e^{i\varphi_{n+1}^{(n)}} |n+1\rangle \right), \\ |\Psi_{n+1}^{(n+1)}\rangle &= \frac{1}{\sqrt{n+1}} \left(e^{i\varphi_1^{(n+1)}} |1\rangle + \dots + e^{i\varphi_n^{(n+1)}} |n\rangle + e^{i\varphi_{n+1}^{(n+1)}} |n+1\rangle \right). \end{aligned} \quad (3.22)$$

By the induction hypothesis, $\{|\Psi_n^{(k)}\rangle\}_{k=1}^n$ generally forms a non-orthogonal basis for the n -dimensional subspace spanned by $\{|1\rangle, \dots, |n\rangle\}$. According to the principles of linear algebra, the n -dimensional component of the $(n+1)$ -th vector can be uniquely decomposed as:

$$\frac{1}{\sqrt{n}} \left(e^{i\varphi_1^{(n+1)}} |1\rangle + \dots + e^{i\varphi_n^{(n+1)}} |n\rangle \right) = \sum_{k=1}^n c_k |\Psi_n^{(k)}\rangle. \quad (3.23)$$

Consequently, $|\Psi_{n+1}^{(n+1)}\rangle$ is linearly dependent on the set $\{|\Psi_{n+1}^{(k)}\rangle\}_{k=1}^n$ if and only if the coefficients $\{c_k\}_{k=1}^n$ satisfy the stringent phase-matching condition:

$$e^{i\varphi_{n+1}^{(n+1)}} = \sum_{k=1}^n c_k e^{i\varphi_k^{(n+1)}}. \quad (3.24)$$

Given that the phases $\{\varphi_k^{(n+1)}\}_{k=1}^{n+1}$ are independently and identically distributed, the probability that this specific equality holds is equal to zero. Therefore, the set $\{|\Psi_{n+1}^{(k)}\rangle_{k=1}^{n+1}\}$ is almost surely linearly independent, completing the proof by induction.

Alternatively, the linear independence of the set $\{|\Psi_n^{(k)}\rangle\}_{k=1}^n$ in Eqs. (3.21) can be established directly by examining the $n \times n$ coefficient matrix M , where the entries are defined as $M_{jk} = \exp(i\varphi_j^{(k)})$. The determinant of M is given by the Leibniz formula:

$$\det(M) = \sum_{\sigma \in S_n} \prod_{i=1}^n M_{i,\sigma(i)} \quad (3.25)$$

where S_n denotes the permutation group of n elements. To prove that $\det(M) \neq 0$ almost surely, we first note that the function $f(\{\varphi_j^{(k)}\}) = \det(M)$ is an analytic function of the phases and is not identically zero. For instance, the phases can be specifically chosen such that M takes the form of a non-singular Vandermonde matrix. According to the property of zeros of analytic functions (e.g. Proposition 1 in Ref. [12]), the set of phases for which $f(\{\varphi_j^{(k)}\}) = \det(M) = 0$ has a measure of zero. Consequently, the random phase vectors are almost surely linearly independent, confirming that the RPS manifold has a dimensionality of n .

4 Chimera-superposition states

4.1 Haar-random construction of unitary ensemble

We now turn to our second construction of the α -random unitary ensemble by leveraging the structure, $U = V\Phi V^\dagger$, where V is a Haar-random unitary drawn uniformly from $SU(D)$, and Φ is a fixed perturbative unitary operation interpolating between V and V^\dagger . This representation captures the essential mechanism by which randomness is introduced through conjugation by a Haar-random unitary, while Φ encodes a controllable deviation from the identity that tunes the strength of the ensemble's randomness.

For an arbitrary unitary operator Φ , one can always express it as an exponential of a Hermitian generator, namely $\Phi = e^{-iH}$, where H is Hermitian. Diagonalizing $H = V_H \Lambda V_H^\dagger$ with the unitary V_H and diagonal Λ , we obtain $\Phi = V_H e^{-i\Lambda} V_H^\dagger$ and hence

$$U = V V_H e^{-i\Lambda} (V V_H)^\dagger. \quad (4.1)$$

A key simplification arises from the invariance of the Haar measure under both left and right multiplication. Since V_H is fixed, the left–right invariance of Haar measure (namely, the product VV_H is distributed identically to V itself) allows us to simplify the ensemble average over U to

$$U = Ve^{-i\Lambda}V^\dagger. \quad (4.2)$$

By exploiting the standard second-moment properties of Haar-random unitaries, we can derive the corresponding first-moment identities for the constructed ensemble,

$$\begin{aligned} \mathbb{E}_{U \sim \mathcal{U}_\alpha}[U_{i_1 j_1} U_{i_2 j_2}^*] &= \mathbb{E}_{V \sim \text{Haar}} \left[(Ve^{-i\Lambda}V^\dagger)_{i_1 j_1} (Ve^{i\Lambda}V^\dagger)_{j_2 i_2} \right] \\ &= \sum_{mn} \mathbb{E}_{V \sim \text{Haar}} [V_{i_1 m} V_{j_2 n} V_{j_1 m}^* V_{i_2 n}^*] e^{i(\Lambda_{nn} - \Lambda_{mm})} \\ &= \frac{|\text{tr}(e^{i\Lambda})|^2 - 1}{D^2 - 1} \delta_{i_1 j_1} \delta_{i_2 j_2} + \frac{1}{D^2 - 1} \left(D - \frac{|\text{tr}(e^{i\Lambda})|^2}{D} \right) \delta_{i_1 i_2} \delta_{j_1 j_2} \\ &= \frac{\alpha D^2 - 1}{D^2 - 1} \delta_{i_1 j_1} \delta_{i_2 j_2} + \frac{D}{D^2 - 1} (1 - \alpha) \delta_{i_1 i_2} \delta_{j_1 j_2} \\ &\approx \alpha \delta_{i_1 j_1} \delta_{i_2 j_2} + \frac{1}{D} (1 - \alpha) \delta_{i_1 i_2} \delta_{j_1 j_2}, \end{aligned} \quad (4.3)$$

where the ensemble parameter α is determined by the normalized spectral form factor (SSF) of the fixed unitary Φ , namely

$$\alpha = \frac{1}{D} |\text{tr}(e^{i\Lambda})|^2 = \frac{1}{D} |\text{tr}(\Phi)|^2. \quad (4.4)$$

Similarly, one can immediately find that these first-moment identities lead to the contraction for an arbitrary quantum operator \mathcal{A} [i.e. Lemma 1 in the main text],

$$\mathbb{E}_{U \sim \mathcal{U}_\alpha}[U^\dagger \mathcal{A} U] = \alpha \mathcal{A} + \frac{(1 - \alpha)}{D} \text{tr}(\mathcal{A}) \mathbb{I}, \quad (4.5)$$

where the second term is a completely depolarization channel resulting from

$$\Delta_{i_1, i_2, j_1, j_2} = \frac{1}{D} \delta_{i_1 i_2} \delta_{j_1 j_2}. \quad (4.6)$$

4.2 Optimal perturbative unitary

Theorem 1 in the main text establishes that the optimal ensemble contraction factor, $\alpha = |\text{tr}(\Phi)|^2/D$, takes the value $1/2$, leading directly to $\mathbb{E}(f_Q) = N/4 + 1/2$ for the QFI density of CSS. We now show how this condition can be realized in a generic N -particle quantum system. Consider each particle to be a spin- J object with local dimension of $d = 2J + 1$, and take $\Phi = e^{-iH}$ as a local perturbation, for instance,

$$H = \chi S_z^{(1)} \otimes \mathbb{I} \otimes \mathbb{I} \cdots \otimes \mathbb{I}, \quad (4.7)$$

where $S_z = \text{diag}[J, J - 1, \dots, -J]$. Under such an assumption, we obtain that

$$\alpha = \left(\frac{\sin \left[\left(J + \frac{1}{2} \right) \chi \right]}{d \sin \left(\frac{\chi}{2} \right)} \right)^2. \quad (4.8)$$

For qubit systems ($J = 1/2$), this reduces to $\alpha = [\cos(\chi/2)]^2$, implying that $\alpha = 1/2$ is achieved at $\chi = \pi/2$. For qutrit ($J = 1$), one finds $\alpha = [1 + 2 \cos(\chi)]^2/9$, yielding $\alpha = 1/2$ at $\chi \approx 55.9^\circ$. The

fixed unitary Φ may also represent a collective rotation. As an illustrative example, we focus on the N -qubit system with $\Phi = e^{-i\chi J_z}$. In this case, the ensemble parameter becomes

$$\alpha = \frac{1}{D} \left| \sum_{m=0}^N C_N^m e^{i(m-\frac{N}{2})\chi} \right|^2 = \left[\cos\left(\frac{\chi}{2}\right) \right]^{\frac{N}{2}}, \quad (4.9)$$

which reaches its optimal value $\alpha = 1/2$ at $\chi = \sqrt{2 \log 2/N} \approx \sqrt{1.4/N}$.

4.3 Chimera-superposition states

In Shchrödinger picture, the metrological states generated by our second α -random unitary ensemble can be decomposed as

$$|\Psi_U\rangle = V\Phi V^\dagger |\Psi\rangle = \sqrt{\alpha} e^{i\beta} |\Psi\rangle + \sqrt{1-\alpha} |\Psi_{\tilde{V}}\rangle, \quad (4.10)$$

where the phase $\beta = \arg(\text{tr}(\Phi))$ and $|\Psi_{\tilde{V}}\rangle = \tilde{V}|\Psi\rangle$ with

$$\tilde{V} = \frac{1}{\sqrt{1-\alpha}} V(\Phi - \sqrt{\alpha} e^{i\beta}) V^\dagger. \quad (4.11)$$

In general, the operator \tilde{V} is no longer unitary. However, by utilizing the first and second moments of Haar-random unitaries, we can obtain that

$$\begin{aligned} \mathbb{E}_{V \sim \text{Haar}}[\tilde{V}_{i_1 j_1}] &= 0 \\ \mathbb{E}_{V \sim \text{Haar}}[\tilde{V}_{i_1 j_1} \tilde{V}_{i_2 j_2}^*] &= \frac{D}{D^2-1} \delta_{i_1 i_2} \delta_{j_1 j_2} - \frac{1}{D^2-1} \delta_{i_1 j_1} \delta_{i_2 j_2} \approx \frac{1}{D} \delta_{i_1 i_2} \delta_{j_1 j_2}, \end{aligned} \quad (4.12)$$

which implies that the zeroth and first moments of \tilde{V} nearly coincide with a Haar-random unitary. Particularly, all rows of \tilde{V} in an average sense are nearly orthogonal to each other,

$$\mathbb{E}_{V \sim \text{Haar}} \left[\sum_j \tilde{V}_{i_1 j} \tilde{V}_{i_2 j}^* \right] \approx \delta_{i_1 i_2}. \quad (4.13)$$

Therefore, \tilde{V} is, on average, approximately a Haar-random unitary up to the first order. These results allows us to find that

$$\mathbb{E}_{V \sim \text{Haar}}[\tilde{V}^\dagger \mathcal{A} \tilde{V}] = \frac{D}{D^2-1} \text{tr}(\mathcal{A}) \mathbb{I} - \frac{1}{D^2-1} \mathcal{A}, \quad (4.14)$$

which implies that the effect of \tilde{V} acting on an arbitrary quantum operator is like a completely depolarization channel given by an exact Haar random unitary when neglecting the second exponentially small term. This directly leads to that

$$\begin{aligned} \mathbb{E}_{V \sim \text{Haar}}[\langle \Psi_{\tilde{V}} | \Psi_{\tilde{V}} \rangle] &= 1, \\ \mathbb{E}_{V \sim \text{Haar}}[|\langle \psi | \Psi_{\tilde{V}} \rangle|^2] &= \frac{1}{D}, \end{aligned} \quad (4.15)$$

where the second equation holds for an arbitrary quantum state $|\psi\rangle$. Therefore, $|\Psi_{\tilde{V}}\rangle$ approximately has a unit norm and an exponentially small overlap with any other fixed quantum state. We denote $|\Psi_{\tilde{V}}\rangle$ as $|\Psi_{\text{H}}^{(1)}\rangle$ in the main text, indicating its first-order resemblance to a genuine Haar-random state. In such a sense, the metrological state in Eq. (4.10) can be viewed as a novel coherent superposition of an ordered state and a highly-random (Haar-like) state. We would like to refer to such states as a class of *Chimera-superposition states* (CSSs).

It is worth pointing out that a Haar-random state typically has an exponentially large state complexity as the system size increase [13, 14]. Consequently, the ordered and random components of $|\Psi_U\rangle$ (namely, $|\Psi\rangle$ and $|\Psi_{\tilde{V}}\rangle$) differ significantly in their state complexity, and cannot be connected by those simple observable operators such as $\mathcal{A} = J_z$ or $\mathcal{A} = J_z^2$. In a mathematically rigorous manner, by utilizing the relation in Eq. (4.14), we can find that

$$\begin{aligned}\mathbb{E}_{V \sim \text{Haar}}[|\langle \Psi | J_z | \Psi_{\tilde{V}} \rangle|^2] &= \Theta\left(\frac{N^2}{D}\right), \\ \mathbb{E}_{V \sim \text{Haar}}[|\langle \Psi | J_z^2 | \Psi_{\tilde{V}} \rangle|^2] &= \Theta\left(\frac{N^4}{D}\right),\end{aligned}\tag{4.16}$$

which is greatly suppressed by the huge dimension, $D = 2^N$, of the Hilbert space. As a result, the expectation values of such observables with respect to $|\Psi_U\rangle$ approximately decompose as

$$\langle \Psi_U | \mathcal{A} | \Psi_U \rangle \approx \alpha \langle \Psi | \mathcal{A} | \Psi \rangle + (1 - \alpha) \langle \Psi_{\tilde{V}} | \mathcal{A} | \Psi_{\tilde{V}} \rangle,\tag{4.17}$$

where the second term in the right-hand side typically makes negligible contribution as compared to the first term. Finally, the expectation values are contracted by a factor of α , consistent with the operator contraction in the Heisenberg picture. Based on Theorem 1 in the main text, the CSSs can efficiently achieve quantum enhanced precision at the Heisenberg-limited scaling. By following a similar analysis, the CSSs in Eq. (4.10) can be generalized to a broader class where $|\Psi_{\tilde{V}}\rangle$ is replaced by a true Haar-random state without compromising the ubiquitous quantum advantage.

Assuming a Hilbert space spanned by the computational basis $\{|b\rangle\}_{b=0}^{D-1}$ with $D = d^N$, we further demonstrate the exponential dimensionality of the following explicit CSS manifold,

$$\mathcal{M} = \{|\Psi_{\text{CSS}}\rangle = |0\rangle + |\Psi_{\text{H}}\rangle\}.\tag{4.18}$$

Here, $|\Psi_{\text{H}}\rangle$ denotes all the Haar-random states, and we neglect the global normalization constant in $|\Psi_{\text{CSS}}\rangle$ for simplicity. Firstly, the intrinsic dimension of the CSS manifold is directly inherited from the underlying Haar-random state $|\Psi_{\text{H}}\rangle$. A general state in a D -dimensional Hilbert space is described by D complex amplitudes. After imposing the unit-norm constraint and subtracting the global phase degree of freedom, the manifold of Haar-random states (the complex projective space $\mathbb{C}P^{D-1}$) possesses a real intrinsic dimension of $2D - 2$. Since the mapping from $|\Psi_{\text{H}}\rangle$ to $|\Psi_{\text{CSS}}\rangle$ is a diffeomorphism and preserves the dimension of the underlying manifolds, the CSS manifold retains the full $2D - 2$ real degrees of freedom and thus has an intrinsic dimension that scales exponentially as $2D - 2$.

Beyond its local dimensionality, we next show that the CSS manifold is also geometrically non-degenerate, meaning its embedding dimension (i.e. dimension of its linear span) is equal to $D = d^N$. To prove this fact, we take D linearly independent Haar-random states $\{|\Psi_{\text{H}}^{(k)}\rangle\}_{k=1}^D$ and establish the linear independence of the corresponding $\{|\Psi_{\text{CSS}}^{(k)}\rangle = |0\rangle + |\Psi_{\text{H}}^{(k)}\rangle\}_{k=1}^D$. Consider the probability measure of existing a set of $\{c_k\}_{k=1}^D$ such that

$$\sum_{k=1}^D c_k \left(|0\rangle + |\Psi_{\text{H}}^{(k)}\rangle\right) = 0.\tag{4.19}$$

Using the unique decomposition of $|0\rangle$ in the basis of $\{|\Psi_{\text{H}}^{(k)}\rangle\}_{k=1}^D$, i.e. $|0\rangle = \sum_{k=1}^D a_k |\Psi_{\text{H}}^{(k)}\rangle$, we can obtain that

$$\sum_{k=1}^D w a_k |\Psi_{\text{H}}^{(k)}\rangle = - \sum_{k=1}^D c_k |\Psi_{\text{H}}^{(k)}\rangle\tag{4.20}$$

where $w = \sum_{k=1}^D c_k$. Hence, $c_k = -wa_k$, which further leads to that $\sum_{k=1}^D a_k = -1$. We point out that by randomly choosing D linearly independent Haar-random states, the probability measure of the decomposition $|0\rangle = \sum_{k=1}^D a_k |\Psi_{\text{H}}^{(k)}\rangle$ satisfying the condition of $\sum_{k=1}^D a_k = -1$ is zero. Therefore, the $\{|\Psi_{\text{CSS}}^{(k)}\rangle\}_{k=1}^D$ can be linearly independent to each other, implying the embedding dimension of the CSS manifold is given by D .

4.4 Concentration of metrological usefulness of CSSs

To establish that most CSS generated by our second construction are metrologically useful, we exploit the concentration-of-measure technique [9]. In the same way, we consider the function returning the expectation value of the operator \mathcal{A} with respect to $|\Psi_U\rangle$,

$$f(V; \mathcal{A}) = \langle \Psi_U | \mathcal{A} | \Psi_U \rangle = \langle \Psi | V \Phi^\dagger V^\dagger \mathcal{A} V \Phi V^\dagger | \Psi \rangle. \quad (4.21)$$

The function $f(V; \mathcal{A}) : \text{SU}(D) \rightarrow \mathbb{R}$ is Lipschitz continuous on the special unitary group. Its Lipschitz norm can be obtained by considering that

$$\left. \frac{d}{d\varphi} f(e^{-i\varphi X} V; \mathcal{A}) \right|_{\varphi=0} = i \langle \Psi | V \Phi^\dagger V^\dagger [X, \mathcal{A}] V \Phi V^\dagger | \Psi \rangle - i \langle \Psi | [X, V \Phi^\dagger V^\dagger \mathcal{A} V \Phi V^\dagger] | \Psi \rangle, \quad (4.22)$$

the magnitude of which is bounded by

$$\begin{aligned} \left| \left. \frac{d}{d\varphi} f(e^{-i\varphi X} V; \mathcal{A}) \right|_{\varphi=0} \right| &\leq \|V \Phi^\dagger V^\dagger [X, \mathcal{A}] V \Phi V^\dagger\|_\infty + \|[X, V \Phi^\dagger V^\dagger \mathcal{A} V \Phi V^\dagger]\|_\infty \\ &\leq \|[X, \mathcal{A}]\|_\infty + 2\|X\|_\infty \|V \Phi^\dagger V^\dagger \mathcal{A} V \Phi V^\dagger\|_\infty \\ &\leq 4\|\mathcal{A}\|_\infty \|X\|_\infty \leq 4\|\mathcal{A}\|_\infty \|X\|_{\text{HS}}. \end{aligned} \quad (4.23)$$

Therefore, the Lipschitz norm of $f(V; \mathcal{A})$ is upper bounded by $\|f\|_{\text{Lip}} \leq 4\|\mathcal{A}\|_\infty$. By *Lévy's lemma*, for any $\epsilon > 0$,

$$\Pr(|f(V; \mathcal{A}) - \mathbb{E}_{\text{Haar}}[f(V; \mathcal{A})]| \geq \epsilon) \leq 2 \exp\left(-\frac{D\epsilon^2}{64\|\mathcal{A}\|_\infty^2}\right), \quad (4.24)$$

This inequality shows that, as the dimension D of the Hilbert space increases, the value of $f(V)$ for a Haar-random V is exponentially concentrated around its mean. Based on Theorem 2 in the main text, the QFI of the CSS manifold associated with the collective generator $\mathcal{O} = \sum_{m=1}^N \mathcal{O}_m$ obeys the following concentration inequality,

$$\Pr(F_Q(|\Psi_U\rangle; \mathcal{O}) < \Theta(N^2)) \leq \exp(-\Theta(D)), \quad (4.25)$$

which immediately implies the Corollary 2.2 in the main text.

4.5 CSS generation by random quantum circuits

The generation of the CSS is based on a simple unitary sandwiched by a Haar-random unitary and its Hermitian conjugate. Although implementing a true Haar-random unitary typically requires exponential experimental resources, the essential feature of our random unitaries that lead to metrological advantage merely depends on their first-moment structures, which are completely determined by second moments of the underlying Haar-random unitaries. This fact allows us to employ several useful approximations [15], such as approximate unitary k -designs and pseudorandom unitaries. Recently, even extremely low depth of random circuits, constructed by gluing small random unitary designs [16], have been proposed. Here, we provide an illustrative example of 2-local random quantum circuits to

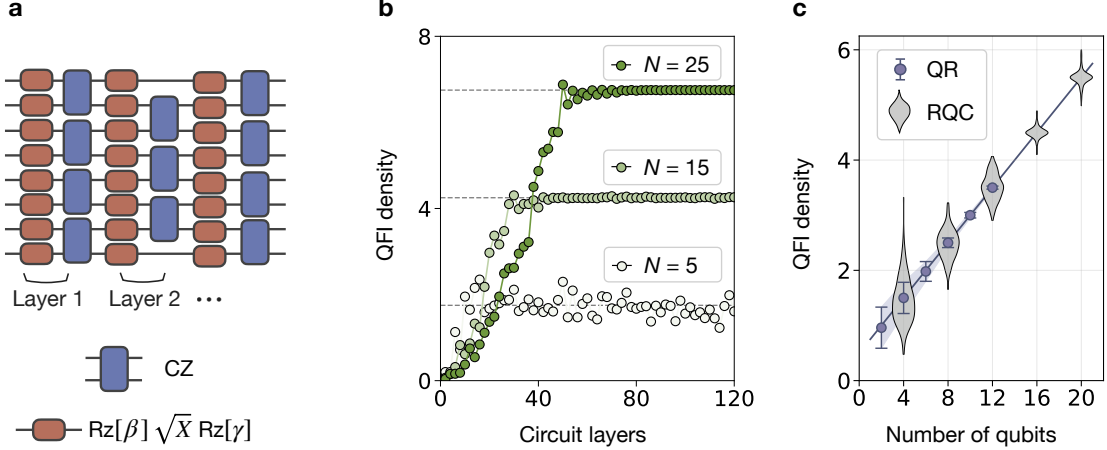


Figure S1: **Generation of CSSs in random local quantum circuits.** **a**, A geometrically local brickwork circuit, alternating single-qubit random rotations (with β, γ uniformly sampled from $[0, 2\pi]$) and CZ gates, is employed to produce approximate Haar-random unitaries. **b**, For a single random instance, the numerically calculated QFI density f_Q of the generated CSS increases with circuit depth and saturate (dashed lines) with negligible fluctuations at large system sizes. **c**, Violin plots of f_Q values, with each from 200 numerical realizations of the random quantum circuit, follow the predicted scaling $\mathbb{E}(f_Q) = N/4 + 1/2$ (dash-dotted line). Filled circles represent the mean f_Q of CSS by using 200 exact Haar-random unitaries from QR decomposition for each qubit number, where the corresponding error bars indicate one standard deviation that swiftly shrink to nearly zero.

implement approximate Haar-random unitaries [see Fig. S1 (a)]. Fig. S1 (b) shows that the QFI density for different system sizes quickly approaches our theoretical prediction given by $\mathbb{E}[f_Q] = N/4 + 1/2$ with increasing circuit depth, signaling the onset of Haar-random statistics in the dynamics. In the saturation regime, the QFI density remains stable with the addition of more layers, particularly for large N . This indicates that the CSSs generated by these approximate Haar-random circuits achieve the expected Heisenberg-limited scaling, with only minor deviations in metrological usefulness at large system sizes. We further confirm such behavior in Fig. S1 (c) by randomly generating a large sample of CSSs. These results support our finding of the concentration-of-measure phenomenon (see Corollary 2.2 in the main text).

4.6 Extension to Gaussian unitary ensemble

We demonstrate that our second α -random unitary ensemble can also be realized through time evolution governed by random Hamiltonians sampled from the Gaussian unitary ensemble (GUE). The GUE is an ensemble of complex Hermitian matrices whose entries are drawn from complex Gaussian distributions. More specifically, if the entries of a random matrix H is denoted as

$$H_{ii} = x_{ii}, \quad H_{ij} = \frac{1}{\sqrt{2}}(x_{ij} + iy_{ij}) \quad \text{for } i < j, \quad (4.26)$$

the GUE requires that $\{x_{ii}, x_{ij}, y_{ij}\}$ obey independent normal distributions, i.e. $\mathcal{N}(0, \sigma^2)$ with σ^2 taken as $1/D$ by convention. Consequently, the probability density function of GUE reads

$$P(H) \propto \exp\left(-\frac{D}{2}\text{tr}(H^2)\right). \quad (4.27)$$

Importantly, random matrices drawn from GUE can be decomposed as

$$H = V\Lambda V^\dagger, \quad (4.28)$$

where V can be viewed as a Haar-random unitary since the distribution of H is unitarily invariant, i.e. $P(H) = P(UHU^\dagger)$ for arbitrary $U \in \text{SU}(D)$. The eigenvalue matrix $\Lambda = \text{diag}[E_1, E_2, \dots, E_D]$ satisfies the following joint probability distribution

$$P(E_1, \dots, E_D) = \frac{1}{Z_D(\sigma)} \prod_{i < j} (E_i - E_j)^2 \exp\left(-\frac{1}{2\sigma^2} \sum_i E_i^2\right), \quad (4.29)$$

where $Z_D(\sigma)$ is a normalization factor. Based on this distribution, the average eigenvalue density of H can be derived as,

$$\rho(E) = \mathbb{E}_{H \sim \text{GUE}} [\hat{\rho}(E)] = \frac{1}{2\pi} \sqrt{4 - E^2} \quad \text{with} \quad \hat{\rho}(E) = \frac{1}{D} \sum_i \delta(E - E_i), \quad (4.30)$$

which is the well-known Wigner's semicircle distribution. Moreover, the joint probability distribution of finding two eigenvalues at E and E' is given by a disconnected piece and a squared sine kernel [17],

$$R(E, E') = \mathbb{E}_{H \sim \text{GUE}} [\hat{\rho}(E)\hat{\rho}(E')] = \frac{D^2}{D(D-1)} \rho(E)\rho(E') - \frac{D^2}{D(D-1)} \frac{\sin^2[D(E-E')]}{[\pi D(E-E')]^2}. \quad (4.31)$$

This two-point correlation function allows us to analytically compute the SSF of the GUE dynamics,

$$\begin{aligned} \mathbb{E} [|\text{tr}(e^{-iHt})|^2] &= \mathbb{E} \left[\sum_{m,n=1}^D e^{-i(E_m - E_n)t} \right] \\ &= D^2 \int e^{-i(E-E')t} R(E, E') dE dE' = D^2 r_1(t)^2 - D r_2(t) + D \end{aligned} \quad (4.32)$$

where $r_1(t) = J_1(2t)/t$ and $r_2(t) = 1 - t/(2D)$ for $t < 2D$.

Realization of the α -random unitary ensemble. The time evolution governed by H drawn randomly from the GUE naturally realize our random unitary ensemble,

$$U(t) = e^{-iHt} = V e^{-i\Lambda t} V^\dagger. \quad (4.33)$$

Applying the same procedures as in Eq. (4.3), we obtain identical first moments for $U(t)$, thus leading to an equivalent operator contraction with a time-dependent ensemble parameter,

$$\alpha(t) = r_1(t)^2 - \frac{1}{D} r_2(t) + \frac{1}{D}. \quad (4.34)$$

As shown in Figure S2, an appropriately chosen evolution time yields an optimal value of $\alpha(t)$, thereby maximizing the ensemble's metrological usefulness.

Concentration-of-measure of GUE dynamics. The concentration-of-measure phenomenon for unitary evolutions generated by GUE Hamiltonians can be rigorously established via the Lipschitz continuity of observables in high-dimensional Gaussian spaces. Consider

$$f(H; \mathcal{A}) = \langle \Psi | e^{iHt} \mathcal{A} e^{-iHt} | \Psi \rangle. \quad (4.35)$$

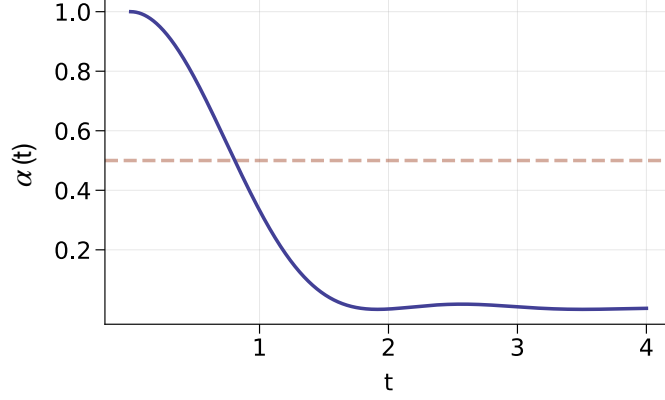


Figure S2: **Time-dependent ensemble parameter from GUE dynamics.** We plot $\alpha(t)$ in Eq. (4.34), which approximately achieves the optimal value (i.e. $\alpha = 1/2$ denoted by the dashed line) at $t = 0.81$.

which quantifies the expectation value of an operator \mathcal{A} under time evolution governed by H . To bound its sensitivity to fluctuations in H , we take advantage of the following inequality,

$$\|U^\dagger \mathcal{A} U - V^\dagger \mathcal{A} V\| = \|(U^\dagger - V^\dagger) \mathcal{A} U + V^\dagger \mathcal{A} (U - V)\| \leq 2\|U - V\| \|\mathcal{A}\|, \quad (4.36)$$

which directly leads to the following Lipschitz bound

$$\begin{aligned} |f(H_1; \mathcal{A}) - f(H_2; \mathcal{A})| &= \left| \langle \Psi | e^{iH_1 t} \mathcal{A} e^{-iH_1 t} - e^{iH_2 t} \mathcal{A} e^{-iH_2 t} | \Psi \rangle \right| \\ &\leq \left\| e^{iH_1 t} \mathcal{A} e^{-iH_1 t} - e^{iH_2 t} \mathcal{A} e^{-iH_2 t} \right\|_\infty \\ &\leq 2\|\mathcal{A}\|_\infty \|D(t)\|_\infty, \end{aligned} \quad (4.37)$$

where $D(t) = e^{-iH_1 t} - e^{-iH_2 t}$. By differentiating $D(t)$, we can obtain

$$\frac{dD(t)}{dt} = -iH_1 D(t) - i(H_1 - H_2) e^{-iH_2 t}, \quad (4.38)$$

which can be further expressed as

$$\frac{d}{dt} \left(e^{iH_1 t} D(t) \right) = -i e^{iH_1 t} (H_1 - H_2) e^{-iH_2 t}. \quad (4.39)$$

The integration then gives

$$D(t) = -i e^{-iH_1 t} \int_0^t e^{iH_1 s} (H_1 - H_2) e^{-iH_2 s} ds = -i \int_0^t e^{-iH_1(t-s)} (H_1 - H_2) e^{-iH_2 s} ds, \quad (4.40)$$

implying

$$\|D(t)\|_\infty \leq t \|H_1 - H_2\|_\infty \leq t \|H_1 - H_2\|_{\text{HS}}. \quad (4.41)$$

The combination of Eqs. (4.37) and (4.41) indicates that the Lipschitz constant of $f(H; \mathcal{A})$ is upper bounded by $L = 2t\|\mathcal{A}\|_\infty$ by noticing that

$$\|H_1 - H_2\|_{\text{HS}}^2 = \sum_i \left(x_{ii}^{(1)} - x_{ii}^{(2)} \right)^2 + \sum_{i \neq j} \left(x_{ij}^{(1)} - x_{ij}^{(2)} \right)^2 + \sum_{i \neq j} \left(y_{ij}^{(1)} - y_{ij}^{(2)} \right)^2. \quad (4.42)$$

Consequently, $f(H; \mathcal{A})$ is governed by the following explicit Gaussian concentration inequality

$$\Pr(|f(H; \mathcal{A}) - \mathbb{E}[f(H; \mathcal{A})]| \geq \epsilon) \leq 2 \exp\left(-\frac{D\epsilon^2}{8t^2\|\mathcal{A}\|_\infty^2}\right). \quad (4.43)$$

Therefore, for physically relevant observables such as $\mathcal{A} \in \{J_z, J_z^2\}$, their expectation values concentrate exponentially around their mean for evolution times $t \ll \sqrt{D}/\text{poly}(N)$. Based on Theorem 2 in the main text, this result further guarantee that almost all states generated by GUE dynamics in this regime are metrologically useful.

Extension to quantum chaotic evolution. Guided by the above analysis in GUE dynamics, it is worth to emphasize that the Haar-random construction of $U = V\Phi V^\dagger$, where V is a Haar-random unitary and Φ encodes a local perturbation (e.g. $\Phi = e^{-i\chi S_z^{(1)}}$ with $S_z^{(1)}$ a local spin operator acting on the first particle), admits a natural dynamical interpretation,

$$U = V\Phi V^\dagger = e^{-i\chi\mathcal{H}}, \quad \mathcal{H} = VS_z^{(1)}V^\dagger. \quad (4.44)$$

Here, \mathcal{H} emerges as a highly non-local random Hamiltonian obtained by conjugating a simple local operator with a Haar-random unitary. This observation provides a transparent physical picture: the seemingly abstract construction $V\Phi V^\dagger$ can be understood as the time evolution generated by a Hamiltonian whose local structure has been thoroughly “scrambled” by a Haar-random unitary. Inspired by such an idea, if V itself arises from the time evolution of a genuinely local (i.e. involving only few-body interactions), chaotic Hamiltonian—i.e., $V = V(t) = e^{-iH_{\text{chaotic}}t}$ —then for times exceeding the scrambling time, \mathcal{H} effectively behaves as a fully non-local operator with spectral properties indistinguishable from those of GUE Hamiltonians [18]. Importantly, this connection provides a concrete bridge between structured random local dynamics and the emergence of GUE random-matrix behavior, reinforcing the physical relevance of our unitary ensemble construction in realistic many-body quantum chaotic systems. These observations open a pathway in platforms such as trapped ions, superconducting qubits, or Rydberg atom arrays, where one can generate chaotic evolution $V(t)$ using local, tunable Hamiltonians and subsequently apply a simple local perturbation Φ to realize our unitary ensembles with controllable $\alpha(t)$. Thus, the metrological advantages predicted by our framework can also, in principle, be observed in near-term quantum devices operating in the prethermal or post-scrambling regimes.

5 Experimental verification of enhanced metrology using ERSs

5.1 RPSs with correlated random phases

Guided by the typical usefulness of RPSs, in this section, we also introduce more easily accessible ERSs in experimental settings—a broader class of RPSs with correlated random phases. Specifically, we construct these states using the following random Hamiltonian ensemble,

$$H = \sum_{(ij) \in e^*} \phi_{ij} \hat{P}_{ij} \quad \text{with} \quad \hat{P}_{ij} \equiv Z_i Z_j - Z_i - Z_j, \quad (5.1)$$

where e^* represents the set of the involved two-body interactions, and all the interaction weights $\{\phi_{ij}\}$ are assumed to obey independent identical normal distributions. All the operators, \hat{P}_{ij} , are diagonal in the computational basis and commute with each other. Physically, the evolution generated by each

\hat{P}_{ij} corresponds to a controlled-phase (CP) gate up to a global trivial phase, namely

$$e^{i\phi_{ij}\hat{P}_{ij}} = e^{-i\phi_{ij}} \text{CP}(4\phi_{ij}) = e^{-i\phi_{ij}} \begin{bmatrix} 1 & 0 & 0 & 0 \\ 0 & 1 & 0 & 0 \\ 0 & 0 & 1 & 0 \\ 0 & 0 & 0 & e^{4i\phi_{ij}} \end{bmatrix}. \quad (5.2)$$

Utilizing the above random Hamiltonians, the realized diagonal random unitaries are given by

$$U = \Phi = e^{iH} = \sum_{b=1}^D e^{i\varphi_b} |b\rangle\langle b|. \quad (5.3)$$

Here, $\{|b\rangle\}_{b=1}^D$ denotes the complete set of the computational basis, and the corresponding random phases $\{\varphi_b\}$ are related to the set of interaction weight parameters $\{\phi_{ij}\}$ by a $D \times |e^*|$ linear transformation matrix,

$$\varphi_b = \sum_{(ij) \in e^*} \phi_{ij} \lambda_{ij}(b), \quad (5.4)$$

where $\lambda_{ij}(b)$ represents the eigenvalue of \hat{P}_{ij} associated with the state $|b\rangle$, i.e. $\hat{P}_{ij} = \sum_{b=1}^D \lambda_{ij}(b) |b\rangle\langle b|$. Crucially, a key distinction arises here: since the Hilbert space dimension is much larger than the number of interaction edges (i.e. $D \gg |e^*|$), the generated random phases $\{\varphi_b\}$ are generally dependent on each other and exhibit statistical correlations, even though the underlying parameters $\{\phi_{ij}\}$ are independent random variables. Therefore, we refer to the ERSs generated by these diagonal random unitaries, i.e. $U = e^{iH}$, as a class of RPS with correlated random phases.

Next, we analytically evaluate the average metrological usefulness of these ERSs generated by $U = e^{iH}$. For generic RPSs, the expectation value for a quantum operator \mathcal{A} is exactly given by,

$$\mathbb{E}[\langle \Psi_U | \mathcal{A} | \Psi_U \rangle] = \frac{1}{2^N} \sum_{a,b} \langle b | \mathcal{A} | a \rangle \mathbb{E} [e^{i(\varphi_a - \varphi_b)}]. \quad (5.5)$$

Below, we focus on the collective spin operators $\mathcal{A} \in \{J_x = \sum_m \sigma_x^{(m)} / 2, J_x^2 = \sum_{m,n} \sigma_x^{(m)} \sigma_x^{(n)} / 4\}$. Notice that the average QFI of $|\Psi_U\rangle$ associated to the Hermitian generator J_x is equal to four times the difference between the following two terms,

$$\begin{aligned} \mathbb{E}[\langle \Psi_U | J_x | \Psi_U \rangle^2] &= \frac{1}{4} \sum_{m,n=1}^N \mathbb{E}[\langle \Psi_U | \sigma_x^{(m)} | \Psi_U \rangle \langle \Psi_U | \sigma_x^{(n)} | \Psi_U \rangle], \\ \mathbb{E}[\langle \Psi_U | J_x^2 | \Psi_U \rangle] &= \frac{1}{4} \sum_{m,n=1}^N \mathbb{E}[\langle \Psi_U | \sigma_x^{(m)} \sigma_x^{(n)} | \Psi_U \rangle]. \end{aligned} \quad (5.6)$$

To determine these quantities, we evaluate each underlying component by expanding these RPSs in the computational basis and averaging over the random phases $\{\varphi_b\}$,

$$\begin{aligned} \mathbb{E}[\langle \Psi_U | \sigma_x^{(m)} | \Psi_U \rangle \langle \Psi_U | \sigma_x^{(n)} | \Psi_U \rangle] &= \frac{1}{4^N} \sum_{a,a',b,b'} \langle a' | \sigma_x^{(m)} | a \rangle \langle b' | \sigma_x^{(n)} | b \rangle \mathbb{E}[e^{i(\varphi_a - \varphi_{a'} + \varphi_b - \varphi_{b'})}], \\ \mathbb{E}[\langle \Psi_U | \sigma_x^{(m)} \sigma_x^{(n)} | \Psi_U \rangle] &= \frac{1}{2^N} \sum_{a,a'} \langle a' | \sigma_x^{(m)} \sigma_x^{(n)} | a \rangle \mathbb{E}[e^{i(\varphi_a - \varphi_{a'})}]. \end{aligned} \quad (5.7)$$

The nonzero contributions in the summation result from the terms of $\langle a' | \sigma_x^{(m)} | a \rangle \langle b' | \sigma_x^{(n)} | b \rangle \neq 0$ and $\langle a' | \sigma_x^{(m)} \sigma_x^{(n)} | a \rangle \neq 0$. For these terms, the associated phase difference $\delta\varphi^{(1)} \equiv \varphi_a - \varphi_{a'} + \varphi_b - \varphi_{b'}$ and $\delta\varphi^{(2)} \equiv \varphi_a - \varphi_{a'}$ further read

$$\begin{aligned}
\delta\varphi^{(1)} &= 2 \sum_{(jm) \in e_G} \phi_{jm} [(-1)^{a_j+a_m} - (-1)^{a_m}] + 2 \sum_{(jn) \in e_G} \phi_{jn} [(-1)^{b_j+b_n} - (-1)^{b_n}]. \\
&= 2 \sum_{(jm) \in e_G \& j \neq n} \phi_{jm} [(-1)^{a_j+a_m} - (-1)^{a_m}] + 2 \sum_{(jn) \in e_G \& j \neq m} \phi_{jn} [(-1)^{b_j+b_n} - (-1)^{b_n}] \\
&\quad + 2\phi_{mn} [(-1)^{a_m+a_n} - (-1)^{a_m} + (-1)^{b_m+b_n} - (-1)^{b_n}], \\
\delta\varphi^{(2)} &= 2 \sum_{(jm) \in e_G \& j \neq n} \phi_{jm} [(-1)^{a_j+a_m} - (-1)^{a_m}] + 2 \sum_{(jn) \in e_G \& j \neq m} \phi_{jn} [(-1)^{a_j+a_n} - (-1)^{a_n}] \\
&\quad - 2\phi_{mn} [(-1)^{a_m} + (-1)^{a_n}],
\end{aligned} \tag{5.8}$$

where the computational basis is explicitly denoted as a N -bit string, e.g. $|a\rangle = |a_1, a_2, \dots, a_N\rangle$. Here, we are interested in quantum correlations between the m -th and n -th qubits for $m \neq n$, which underpins the metrological potential of $|\Psi_U\rangle$ to surpass the standard quantum limit. By taking advantage of statistical independence between $\{\phi_{ij}\}$, we obtain that

$$\begin{aligned}
\mathbb{E}[e^{i\delta\varphi^{(1)}}] &= \prod_{(jm) \in e_G \& j \neq n} \mathbb{E} \left[e^{2i\phi_{jm} [(-1)^{a_j+a_m} - (-1)^{a_m}]} \right] \times \prod_{(jn) \in e_G \& j \neq m} \mathbb{E} \left[e^{2i\phi_{jn} [(-1)^{b_j+b_n} - (-1)^{b_n}]} \right] \\
&\quad \times \mathbb{E} \left[e^{2i\phi_{mn} [(-1)^{a_m+a_n} - (-1)^{a_m} + (-1)^{b_m+b_n} - (-1)^{b_n}]} \right],
\end{aligned} \tag{5.9}$$

and

$$\begin{aligned}
\mathbb{E}[e^{i\delta\varphi^{(2)}}] &= \prod_{(jm) \in e_G \& j \neq n} \mathbb{E} \left[e^{2i\phi_{jm} [(-1)^{a_j+a_m} - (-1)^{a_m}]} \right] \times \prod_{(jn) \in e_G \& j \neq m} \mathbb{E} \left[e^{2i\phi_{jn} [(-1)^{a_j+a_n} - (-1)^{a_n}]} \right] \\
&\quad \times \mathbb{E} \left[e^{-2i\phi_{mn} [(-1)^{a_m} + (-1)^{a_n}]} \right].
\end{aligned} \tag{5.10}$$

By further assuming that each random interaction weight satisfies $\mathbb{E}[e^{\pm 4\phi_{ij}}] = \delta$ and utilizing a star configuration of e^* , e.g. $e^* = \{(1m)\}_{m=2}^N$, we find that for $m \neq n > 1$,

$$\begin{aligned}
\mathbb{E}[\langle \Psi_U | \sigma_x^{(m)} | \Psi_U \rangle \langle \Psi_U | \sigma_x^{(n)} | \Psi_U \rangle] &= \frac{1}{4}(1 + \delta)^2, \\
\mathbb{E}[\langle \Psi_U | \sigma_x^{(m)} \sigma_x^{(n)} | \Psi_U \rangle] &= \frac{1}{2}(1 + \delta^2).
\end{aligned} \tag{5.11}$$

For small values of δ by assuming large statistical fluctuations of the interaction weights in Eq. (5.1), the average QFI of the generated RPSs with correlated random phases is given by

$$\mathbb{E}[F_Q] = \frac{1}{4}N^2 + O(N). \tag{5.12}$$

5.2 Enhanced metrology with ERSs using trapped ions

We implemented ERS-enhanced quantum metrology on IonQ's Forte-1 trapped-ion platform. The device exhibits all-to-all qubit connectivity, single- and two-qubit gate errors of 0.02% and 0.87%, state-preparation-and-measurement (SPAM) error of 0.44%, coherence times of $T_1 = 100$ s and $T_2 = 1$ s, and average native gate durations of 130 μ s (1Q) and 970 μ s (2Q); see Table S1.

Connectivity	all-to-all	SPAM Error	0.44%	1Q Gate Time	130 μs
1Q Gate Error	0.02%	T1	100 s	2Q Gate Time	970 μs
2Q Gate Error	0.87%	T2	1s	Reset Time	50 μs

Table S1: Performance metrics of IonQ’s Forte-1 trapped-ion quantum processor (recorded on 20 October 2025).

To generate ERSs, we utilize random quantum circuits (RQCs) as shown in Figure 2 of the main text. Specifically, we implement random unitaries of the form $U = V e^{iH} V^\dagger$ on the initial state $|0\rangle^{\otimes N}$, where H is given by Eq. (14) in the main text and $V = \exp(i\pi J_y/2)$. The circuits consist of a local-rotation stage followed by an entangling stage: First, each qubit is initialized in $|+\rangle$ by performing a single-qubit $\text{Ry}[\pi/2]$ rotation. Next, a sequence of controlled-phase gates, $\text{CP}_{1j} \equiv \text{CP}[4\phi_{1j}] = \text{diag}[1, 1, 1, e^{4i\phi_{1j}}]$, is then applied to generate pairwise couplings between the first qubit and qubits $j = 2$ to N . We note that such RQCs are further automatically transpiled into hardware-executable circuits according to the native gate set of IonQ’s Forte-1 processor (i.e. GPI, GPI2 and ZZ gates). After a ERS is prepared, the external signal is encoded as a collective phase shift $e^{i\vartheta J_z}$ with ϑ the parameter to be estimated. We then apply a time-reversed circuit U^\dagger to map the accumulated phase onto a measurable population signal. Specifically, the phase ϑ is inferred from the return probability to the initial state,

$$P(\vartheta) = |\langle \mathbf{x} | e^{-iH} e^{-i\vartheta J_x} e^{iH} | \mathbf{x} \rangle|^2 = |\langle \mathbf{0} | U^\dagger e^{-i\vartheta J_z} U | \mathbf{0} \rangle|^2. \quad (5.13)$$

We test three distinct RQCs, with their corresponding interaction weight parameters listed in Table S2. For each RQC, the phase ϑ is varied from 0 to 0.5 and discretized into 50 evenly spaced points, where each point is obtained from an average over 100 experimental shots. The recorded probability data are fitted using the function

$$P(\vartheta) = A e^{-b\vartheta} \cos(c\vartheta + d) + B, \quad (5.14)$$

from which we estimate the value of ϑ from the regions where the fitted curve has a large slope.

$\phi^{(i)}$	ϕ_{12}	ϕ_{13}	ϕ_{14}	ϕ_{15}	ϕ_{16}	ϕ_{17}	ϕ_{18}	ϕ_{19}	$\phi_{1,10}$
$\phi^{(1)}$	-1.283	0.275	0.308	-0.275	-0.223	0.210	0.204	0.747	-0.800
$\phi^{(2)}$	-0.277	-0.225	-0.175	0.272	-1.240	-0.188	0.198	0.749	-0.262
$\phi^{(3)}$	0.292	0.239	-0.807	-0.717	-0.734	0.660	-0.229	-0.232	0.189

Table S2: Three sets of interaction weight parameters used to generate 10-qubit ERSs in RQCs.

The measurement uncertainty in ϑ due to the quantum projection noise associated with measuring $P(\vartheta)$ can be evaluated as

$$\delta\vartheta^2 = \frac{P(\vartheta)[1 - P(\vartheta)]}{|\partial_\vartheta P(\vartheta)|^2}, \quad (5.15)$$

which provides a lower bound on the QFI density of the experimentally generated ERSs via the quantum Cramér–Rao bound, i.e. $N f_Q \geq \delta\vartheta^{-2}$. The corresponding metrological gain beyond the SQL is estimated in decibels as $20 \log_{10}(\delta\vartheta_{\text{SQL}}/\delta\vartheta) = 20 \log_{10}(\delta\vartheta^{-1} N^{-1/2})$ [19].

References

- [1] S. L. Braunstein and C. M. Caves, *Phys. Rev. Lett.* **72**, 3439 (1994).
- [2] P. Hauke, M. Heyl, L. Tagliacozzo, and P. Zoller, *Nat. Phys.* **12**, 778 (2016).

- [3] Y. Chu, X. Li, and J. Cai, *Phys. Rev. Lett.* **133**, 110201 (2024).
- [4] P. Zanardi and N. Paunković, *Phys. Rev. E* **74**, 031123 (2006).
- [5] A. Niezgoda and J. Chwedeńczuk, *Phys. Rev. Lett.* **126**, 210506 (2021).
- [6] M. Gärttner, P. Hauke, and A. M. Rey, *Phys. Rev. Lett.* **120**, 040402 (2018).
- [7] J. Smith, A. Lee, P. Richerme, B. Neyenhuis, P. W. Hess, P. Hauke, M. Heyl, D. A. Huse, and C. Monroe, *Nat. Phys.* **12**, 907 (2016).
- [8] J.-Y. Desaulles, F. Pietracaprina, Z. Papić, J. Goold, and S. Pappalardi, *Phys. Rev. Lett.* **129**, 020601 (2022).
- [9] G. W. Anderson, A. Guionnet, and O. Zeitouni, *An Introduction to Random Matrices* (Cambridge University Press, Cambridge, 2009).
- [10] M. Ledoux, *The Concentration of Measure Phenomenon* (American Mathematical Society, 2001).
- [11] M. Oszmaniec, R. Augusiak, C. Gogolin, J. Kolodynski, A. Acin, and M. Lewenstein, *Phys. Rev. X* **6**, 041044 (2016).
- [12] B. S. Mityagin, *Math. Notes* **107**, 529 (2020).
- [13] S. Aaronson, Y. Atia, and L. Susskind, [arXiv:2009.07450](https://arxiv.org/abs/2009.07450) (2020).
- [14] A. R. Brown, *Nat. Phys.* **19**, 401 (2023).
- [15] F. G. S. L. Brandão, A. W. Harrow, and M. Horodecki, *Comm. Math. Phys.* **346**, 397 (2016).
- [16] T. Schuster, J. Haferkamp, and H.-Y. Huang, *Science* **389**, 92 (2025).
- [17] J. Cotler, N. Hunter-Jones, J. Liu, and B. Yoshida, *J. High Energy Phys.* **2017**, 48.
- [18] L. Erdős and D. Schröder, *Math. Phys. Anal. Geom.* **17**, 441 (2014).
- [19] Q. Liu, L.-N. Wu, J.-H. Cao, T.-W. Mao, X.-W. Li, S.-F. Guo, M. K. Tey, and L. You, *Nat. Phys.* **18**, 167 (2022).